Personalized Cancer Therapy Prioritization Based on Driver Alteration Co-occurrence Patterns

Lidia Mateo[1], Miquel Duran-Frigola[1], Albert Gris-Oliver[2], Marta Palafox[2], Maurizio Scaltriti[3,4], Pedram Razavi[3,5], Sarat Chandarlapaty[3,5], Joaquin Arribas [6,7,8,9], Meritxell Bellet[10,11], Violeta Serra[2,9] and Patrick Aloy[1,8,*]

[1] Joint IRB-BSC-CRG Program in Computational Biology, Institute for Research in Biomedicine (IRB Barcelona), The Barcelona Institute of Science and Technology, Barcelona, Catalonia, Spain.

[2] Experimental Therapeutics Group, Vall d'Hebron Institute of Oncology, Barcelona, Catalonia, Spain.

[3] Human Oncology and Pathogenesis Program, Memorial Sloan Kettering Cancer Center (MSKCC), New York, NY 10065, USA.

[4] Department of Pathology, MSKCC, New York, NY 10065, USA.

[5] Breast Medicine Service, Department of Medicine, MSKCC and Weill-Cornell Medical College, New York, NY 10065, USA.

[6] Growth Factors Laboratory, Vall d'Hebron Institute of Oncology, Barcelona, Catalonia, Spain.

[7] Department of Biochemistry and Molecular Biology, Universitat Autònoma de Barcelona, Bellaterra, Catalonia, Spain.

[8] Institució Catalana de Recerca i Estudis Avançats (ICREA), Barcelona, Catalonia, Spain.

[9] CIBERONC, Barcelona.

[10] Breast Cancer Group, Vall d'Hebron Institute of Oncology, Barcelona, Catalonia, Spain.

[11] Department of Medical Oncology, Hospital Vall d'Hebron, Universitat Autònoma de Barcelona, Barcelona, Catalonia, Spain.

* Corresponding author: patrick.aloy@irbbarcelona.org

Keywords: Drug-response biomarkers, driver co-occurrence networks, precision oncology.

Abstract

Molecular profiling of personal cancer genomes, and the identification of actionable vulnerabilities and drug-response biomarkers, are the basis of precision oncology. Tumors often present several driver alterations that might be connected by cross-talk and feedback mechanisms, making it difficult to mark single oncogenic variations as reliable predictors of therapeutic outcome. In the current work, we uncover and exploit driver alteration co-occurrence patterns from a recently published *in vivo* screening in patient-derived xenografts (PDXs), including 187 tumors and 53 drugs. For each treatment, we compare the mutational profiles of sensitive and resistant PDXs to statistically define Driver Co-Occurrence (DCO) networks, which capture both genomic structure and putative oncogenic synergy. We then use the DCO networks to train classifiers that can prioritize, among the available options, the best possible treatment for each tumor based on its oncogenomic profile. In a cross-validation setting, our drug-response models are able to correctly predict 66% of sensitive and 77% of resistant drug-tumor pairs, based on tumor growth variation. Perhaps more interesting, our models are applicable to several tumor types and drug classes for which no biomarker has yet been described. Additionally, we experimentally

validated the performance of our models on 15 new tumor samples engrafted in mice, achieving an overall accuracy of 75%. Finally, we adapted our strategy to derive drug-response models from continuous clinical outcome measures, such as progression free survival, which better represent the data acquired during routine clinical practice and in clinical trials. We believe that the computational framework presented here could be incorporated into the design of adaptive clinical trials, revealing unexpected connections between oncogenic alterations and increasing the clinical impact of genomic profiling.

Background

In light of the complexity and molecular heterogeneity of tumors, clinical and histopathological evaluation of cancer patients is nowadays complemented with genomic information. Genome-guided therapy has been shown to improve patient outcome [1, 2] and clinical trial success rate [3] and, despite some controversy [4], prospective molecular profiling of personal cancer genomes has enabled the identification of an increasing number of actionable vulnerabilities [5].

Cancer genome sequencing initiatives have found that any given tumor contains from tens to thousands of mutations. However, only a few of them confer a growth advantage to cancer cells, driving thus the tumorigenic process. The most comprehensive study of 'driver' genes published to date has analyzed over 9,000 tumor samples, across 33 tissues of origin, and has systematically identified driver mutations in 258 genes [6]. Approximately half (142) of those driver genes were associated with a single tumor type, whereas 87 genes seem to provide a growth advantage in several tumor types. The number of drivers detected per tumor type varies widely, ranging from 2 in kidney chromophobe cancer to 55 in uterine cancer. Despite the large number of drivers identified per tumor type, every patient has a unique combination of mutations and copy number variants: ninety percent of patients show at least one putative driver alteration, but each sample only contains a median of three putative altered drivers [7].

On top of identifying key alterations in tumor development, it is fundamental to pinpoint those that can shed light on the most appropriate therapy to treat each tumor (i.e. biomarkers). Often, patients with similar clinicopathological characteristics might be molecularly different [6], this inter-patient heterogeneity is one of the reasons why only a subset of them will actually respond to a given targeted treatment. Computational studies suggest that up to 90% of patients may benefit from molecularly-guided therapy when biomarkers of uncertain clinical significance, as well as off-label and experimental drugs, are used to guide treatment selection [7, 8]. Although randomized controlled trials are still considered the gold standard in the clinics, they cannot address all possible patient clinicopathologic and molecular subtypes [9]. Precision medicine has prompted the reconsideration of clinical drug development pipelines, with the implementation of more sophisticated clinical trial designs, such as umbrella, basket, and platform trials to account for inter-patient heterogeneity [10]. In particular, the implementation of adaptive enrichment strategies allows for continual learning and modification of the eligibility criteria as data accumulate, with the objective of recruiting those patients that are most likely to benefit

from treatment [9-12]. However, despite the implementation of these novel experimental designs, currently only alterations in 25 genes have accumulated enough clinical evidence to be approved as biomarkers by the FDA [13]. Indeed, a recent comprehensive analysis of 6,729 pan-cancer tumors could only identify actionable mutations with therapeutic options available in clinical practice (FDA-approved or international guidelines) or reported in late phase (III–IV) clinical trials in 5.2% and 3.5% of the samples, respectively [14]. These figures coincide with clinical trial enrolment rates [1], where only 89 out of 1,640 of patients could enter genotype-matched treatment trials, the vast majority of which involved mutations in four genes, namely *PIK3CA*, *KRAS*, *BRAF* and *EGFR*. This highlights an acute need to expand the current repertoire of response biomarkers to cover more drugs and patients.

The eligibility criteria of most genomically-matched basket clinical trials are based on the single-gene biomarkers. However, most tumors do not present a single actionable mutation but have co-occurring driver alterations that might simultaneously alter key players of signaling pathways connected by cross-talk and feedback mechanisms [15, 16]. There are many documented cases of functionally relevant co-occurring oncogenic mutations, such as the concomitant inactivation of *TP53* and *RB1* [17], co-deletion of *CDKN2A* and *CDKN2B [18]*, co-amplification of *MDM2* and *CDK4* [19, 20], 1p/19q co-deletion in glioma [21], *MYC* amplification and *TP53* mutations [22] or activating alterations in *KRAS* and *BRAF [5].* At pathway level, the concomitant activation PI3K signaling pathway with FGF signaling (*FGFR2* and *FGFR3*), or with *NRF2* mediated oxidative response have also been identified in several tumor types [16]. In this context, a single-gene based stratification of patients into subtypes and treatment arms might be over-simplistic, and novel frameworks that exploit co-mutational patterns might prove more effective.

As in the identification of driver mutations, the discovery of drug response biomarkers requires large numbers of patient molecular profiles matched to treatment outcomes. Unfortunately, treatment history information of large-scale genomics endeavors has not been systematically collected (e.g. TCGA [23]) or is not yet publicly available (e.g. GENIE Consortium [24]). Even though better data sharing policies are needed, many concerns are raised regarding privacy, property and the preliminary nature of confidential biomedical data. Safer alternative ways of sharing biomedical data are already on the table [25] but, until the access to systematically annotated clinical records becomes a reality, the research community largely relies on drug response data gathered from pre-clinical models.

Cancer cell lines are the most widely used *in vitro* model system, and have been fundamental tools to set the grounds of our understanding of cancer biology and to assess the efficacy of a broad spectrum of cancer drugs [26]. Unfortunately, cancer cell lines have been cultured as monolayers on plastic surfaces, and in growth-promoting conditions, for decades. As a consequence, most of them have suffered a substantial transcriptional drift, and they likely represent a cell subpopulation from the original primary tumor [27]. Those facts have fueled the debate regarding how well cancer cell lines resemble the tumors from which they were established and to which extent they are clinically relevant [15, 27]. A more realistic model to bridge the bench-to-bedside gap is the patient-derived mouse xenograft (PDX) [28]. To some extent, PDXs preserve inter- and intra-tumoral heterogeneity, and mimic the clinical course of the disease and response to targeted therapy, at least in certain

tumor types [29-31]. Indeed, a recent review reported a 91% (153 out of 167) correspondence between the clinical responses of patients and their cognate PDXs [32]. Although this data are more time-intensive and expensive to generate, it is still feasible to establish large *in vivo* screenings, covering a wide diversity of tumor types and drugs. PDXs are thus a clinically relevant platform for pre-clinical pharmacogenomic studies, and represent a more accurate approach to identify predictive biomarkers compared with the use of cancer cell lines [33].

Here, we present a computational strategy to uncover and exploit driver alteration co-occurrence patterns in PDXs. By comparing the molecular profiles of sensitive and resistant PDXs to a given drug, we identify driver co-occurrence networks and use them as a new type of drug-response indicators, applicable much beyond known biomarkers. We apply our strategy to the largest panel of PDXs and drugs available to date [28], and prospectively validate our findings *in vivo*. Finally, we adapt our strategy to derive response predictive models directly from continuous clinical outcome measures, such as progression free survival, and evaluate them on a cohort of breast cancer patients.

Results and Discussion

Driver co-occurrence networks of drug response

Although thousands of genomic profiles of patient tumors are available, accurate information about pharmacological interventions and treatment outcome has not been systematically collected [23], or has not been disclosed yet [24]. Thus, to bypass these limitations, we compiled drug response data obtained in PDXs, since they preserve the overall molecular profile of the original tumor, and maintain its cellular and histological structure [32]. In particular, we based our study on 375 PDXs for which somatic mutations and copy number alterations have been characterized, together with their response to 62 treatments across six indications, using the 'one animal per model per treatment (1x1x1)' experimental design [28]. As suggested by the authors, we adopted the Modified Response Evaluation Criteria in Solid Tumors (mRECIST) [28, 34] to assess the change in tumor volume in response to treatment. We considered to be 'sensitive' those PDXs that showed a Complete Response (CR), Partial Response (PR) or Stable Disease (SD), and 'resistant' those with a Progressive Disease (PD) status.

Of the 62 drugs and drug combinations tested, we selected 53 treatment arms that showed significant inter-individual heterogeneity (i.e. a sufficient number of 'sensitive' and 'resistant' tumors) to model drug response. In total, these data comprised 3,127 experiments performed on 187 PDXs [28] for which we had, at least, 5 sensitive and 5 resistant PDXs. First, we assessed whether this set of PDXs is representative of the genomic diversity observed in human tumors by comparing their alterations to the oncogenomic profiles extracted from 13,719 cancer patients [35]. We found that the 187 PDXs considered broadly covered the whole oncogenomic landscape represented by the full cohort ('PanCancer' cohort in Figure 1). When analyzing tumor types individually, we observed that, while the mutational diversity of some of them is perfectly reflected in the PDX

samples (e.g. colorectal and cutaneous melanoma tumors), the distribution of mutated genes showed clear differences in others (e.g. pancreatic cancer). Overall, there are PDXs representing the most populated areas of the PanCancer cohort, suggesting that the full collection of PDXs may be used in downstream analyses.

We used the Cancer Genome Interpreter [14] to filter out passenger mutations from PDX profiles, and only worked with driver somatic mutations and copy number alterations. For each treatment, we grouped sensitive and resistant PDXs, irrespective of the origin of their tumors. We then identified driver alterations that were overrepresented in sensitive or resistant PDXs, as well as pairs of driver alterations showing statistically significant patterns of co-occurrence in each subpopulation (see *Materials and Methods* for details). Finally, for each treatment, we built a Driver Co-Occurrence (DCO) network in sensitive PDXs consisting of overrepresented drivers (nodes) and pairs of co-occurring drivers (edges), another DCO network for resistant PDXs, and a third general one consisting of all drivers and co-occurrences associated with both treatment responses (Figure 2A). DCO networks for each of the 53 drugs are detailed in Table S1 and can be visualized using Cytoscape [36] (Supplementary Data S1). The total number of drivers and driver co-occurrences captured in the DCO networks varied substantially among treatments, ranging from 28 to 196 driver genes (median of 109 nodes, IQR: 82-136) and 20 to 1,499 pairs of drivers (median of 300 edges, IQR: 220-471) overrepresented in PDXs treated with Ruxolitinib+Biminetinib and the tankyrase inhibitor LJC049, respectively. However, when considering individual animals, the number of altered drivers and pairs of drivers was small and remained quite stable across treatments, with a median of only 9 genes (IQR: 5-15) and 7 driver co-occurrences (IQR: 2-29) per PDX (Figure 2B).

We next sought to assess the novelty of our DCO networks by comparing the overrepresented driver genes, and the co-occurring pairs, to the set of annotated response/resistance biomarkers for each treatment [14]. Figure 2C shows that, although there is some overlap, our approach vastly expands the set of genes to be considered in downstream treatment prioritization applications. More specifically, 47 of the 58 genes annotated as approved or experimental response biomarkers are present in at least one DCO network, and 28 of them are related to the same drug or drug class. Additionally, our DCO networks include 331 novel genes that might be associated to treatment sensitivity or resistance.

Exploring the functional relevance of DCO networks

Even in targeted therapies, where the drugs are rationally designed to modulate well-characterized oncogenic alterations (e.g. *HER2* amplification or the $BRAF^{V600}$ mutation), it is known that alterations in other proteins do also influence drug response. For example, activating alterations in the MAPK or in PI3K/AKT pathways have been related to resistance to BRAF inhibition [37]. We thus explored the functional relationship between the inferred DCO networks and the suggested mechanisms of action of each treatment through the analysis of the ten main oncogenic signaling pathways [16].

As expected, we find that approved or experimental biomarkers of drug response are

directly related to the pathways where their intended targets belong (Fisher's exact test odds-ratio (OR) 5.14, p-value $1.4 \cdot 10^{-8}$). On the other hand, the genes in the DCO networks inferred for each treatment, while keeping certain functional coherence with the therapeutic targets (OR 1.59, p-value 0.090), show a larger functional diversity (Figure 3A, Table S2). For instance, we found that the DCO networks derived in response to tamoxifen are enriched in RTK/RAS/MAPK signaling proteins (OR 2.70, p-value 0.006; see Figure 3A and Table S2). When we analyzed separately sensitive and resistant DCO networks we found that the RTK/RAS/MAPK pathway, which is known to mediate resistance to this therapy [38], is indeed only overrepresented in the resistance DCO network (OR 3.08, p-value 0.004). Interestingly, other DCO networks are enriched in pathways not directly related to the known mechanism of action of the drug (e.g. 5FU, Cetuximab or LJC049, see Figure 3A and Table S2). However, the most striking observation is that cell cycle related proteins seem to play a central role in the inferred DCO networks for more than half of the treatments (35 of 53), irrespectively of the mechanism of action of the drug administered. This trend is not apparent when considering differentially altered drivers alone (Figure 3A).

Beyond the main oncogenic pathways, topological analysis of DCO networks revealed several large, strongly connected modules, composed of driver genes that had been co-amplified or co-deleted as part of the same genomic segment. To account for this effect, we clustered driver genes that are close in the genome and show similar alteration patterns (*Materials and Methods*; Supplementary Figure S2). After the filtering, we could still recapitulate known cases of co-amplification and simultaneous overexpression of adjacent oncogenes shown to provide a cellular cross-talk between tumorigenic pathways. For instance, in the ribociclib (LEE011) + encorafenib, dacarbazine, sonidegib (LDE225), LGW813 (an IAP inhibitor), and TAS266 (a DR5 agonist) DCO networks, we find links between *MDM2* and *CDK4*, which are frequently co-altered as part of the same amplicon in the 12q chromosomal region [19, 20]. Indeed, their hypothetical cooperation has triggered the use of *CDK4/6* inhibitors as potentiators of *MDM2* antagonists [20], which are currently being tested to treat liposarcoma in clinical trials (NCT02343172 and NCT01692496). Another example is the concomitant amplification of *ERBB2* and *TOP2A* as part of the 7q12 amplicon, which occurs in 40–50% of breast cancers [39] and provides a rational basis for the addition of anthracyclines targeting *TOP2A* as adjuvant chemotherapy in the treatment of HER2-positive breast cancer [40]. However, the addition of doxorubicin to the standard regimen can potentially increase cardiotoxicity and failed to demonstrate a significant clinical improvement with respect to trastuzumap+paclitaxel in a phase III trial [41], suggesting that further clinical evaluation is still needed.

DCO networks do not only capture genome structure, but also functional relationships between oncogenic alterations found far apart in the genome. For instance, we observed that PDXs treated with the CDK4/6 inhibitor ribociclib show a markedly reduced response rate when they have co-occurring alterations in *CCND2* and *TP53* (27%, 3 out of 11) compared to PDXs with alterations in *TP53* alone (41%, 29 out of 70) or wild-type *TP53* and *CCND2* (43%, 39 out of 90). Interestingly, alterations in *TP53-CCND2* also tend to co-occur in a large collection of 74,247 pan-cancer samples compiled from 240 cancer studies [42], with *TP53-CCND2* being co-altered in approximately 1% of the samples (751 patients, OR 2.57, p-value < 0.001). In particular, *TP53-CCND2* alterations significantly co-occur in three

out of five tumor-type specific cohorts: in 2,173 breast cancer patients (METABRIC, OR > 8, p-value < 0.001), in 479 patients with skin cutaneous melanoma (TCGA, OR 6.47, p-value 0.01), and in 507 patients with lung adenocarcinoma (TCGA, OR 5.24, p-value 0.015). However, we found no evidence of *TP53-CCND2* co-occurrence in patient cohorts of other tumor types, such as colorectal adenocarcinoma (220 samples from TCGA), or pancreatic adenocarcinoma (175 samples from TCGA). Although the role of *TP53* status in response to CDK4/6 inhibition is controversial [43, 44], *TP53* loss is thought to reduce the expression of its target p21CIP1 (*CDKN1A*) and consequently relieve *CDK2* from its inhibition. On the other hand, cyclin D2 (*CCND2*) preferentially activates *CDK2*, although it can also activate *CDK4 [45]*. Thus, based on our observations and the available literature, we hypothesize that concomitant oncogenic alterations in *TP53* and *CCND2* could shift the CDK4/6 dependency towards an alternative *CDK2*-dependent activation of G1/S transition, rendering those tumors insensitive to CDK4/6 inhibition (Figure 3B).

PIK3CA-mutant tumors are sensitive to isoform-selective PI3K inhibitors such as alpelisib (a) [46-48]. However, *PIK3CA*-independent mechanisms of PI3K activation (e.g. activating alterations in *PIK3CB* or *PTEN* loss) often confer resistance to this treatment [49, 50]. The alpelisib DCO network contains four proteins involved in PI3K signaling, namely *PIK3CA*, *PIK3R1*, *PIK3C2B* and *PTEN*. Indeed, we observed a higher response rate (65%, 15 out of 23) among PDXs with oncogenic *PIK3CA* alterations compared to PDXs with wild-type *PIK3CA* (44%, 52 out of 117), which agrees with the mechanism of action of alpelisib. More interestingly, we found that *PIK3CA*-altered PDXs having no co-occurring oncogenic alterations in the PI3K pathway (n=23) showed an even higher response rate (83 %, 10 out of 12) than those with co-occurring alterations in *PIK3R1*, *PIK3C2B* or *PTEN* (45%, 5 out of 11). These co-occurring alterations likely activate PI3K signaling in a *PIK3CA*-independent manner, hence the limited response to alpelisib[50] (Figure 3C). Out of the three genes co-altered with *PIK3CA*, only *PIK3C2B* is found co-altered more often than expected in PDXs treated with alpelisib (4.06% inferred co-occurrence rate vs. 1.50% expected; expected value of the difference (e-value) 0.006), and we indeed observed that PDXs with *PIK3CA-PIK3C2B* co-alteration showed a lower response rate (33%, 2 out of 6) than those with *PIK3CA* alteration alone (76%, 13 out of 17). Finally, *PIK3CA* and *PIK3C2B* alterations also co-occur in approximately 1% of the 74,247 pan-cancer samples (758 patients, OR 2.99, p-value < 0.001), being particularly co-altered in breast cancer patients (METABRIC, OR 1.48, p-value < 0.001) and pancreatic adenocarcinoma patients (TCGA, OR > 8, p-value 0.002).

Overall, DCO networks capture co-occurring alterations associated to drug resistance in PDXs, as illustrated by the concomitant alteration of *CCND2-TP53* in relation to CDK4/6 inhibition and that of *PIK3CA-PIK3C2B* in relation to PI3K inhibition. Moreover, many of these co-occurrence patterns are also found in patient cohorts, indicating a potential clinical translation of these findings.

TCT4U: A collection of 53 drug response classifiers for genome-driven treatment prioritization

We then explored whether the sets of differentially (co-)altered genes in sensitive and

resistant PDXs can be used to predict drug response. For each treatment, we used the DCO networks to statistically classify PDXs as resistant or sensitive. The goal of this exercise is to identify, among the available treatments, the best possible option for each individual based on its oncogenomic profile. We thus named the set of developed drug response classifiers Targeted Cancer Therapy for You (TCT4U).

In brief, for each treatment arm, we combined the probabilities assigned by three Naïve Bayes (NB) classifiers, trained with sensitivity, resistance and general DCO networks, into a single prediction score per drug-PDX pair. Figure 4A shows the performance of the NB classifiers in a leave-one-out cross-validation setting, whereby the oncogenomic profile of PDXs is used to predict response to each treatment. Additionally, to increase the clinical translatability of our approach, we repeated the calculations considering only those alterations detectable by the Memorial Sloan Kettering-Integrated Mutation Profiling of Actionable Cancer Targets (MSK-IMPACT) [51, 52] and the Foundation Medicine (FM) gene panels [53], which contain probes to detect 410 and 287 mutated genes, respectively, and are widely used in clinical settings. Finally, we assessed the effectiveness of TCT4U by comparing its predictive power to that of FDA-approved and experimental biomarkers (see *Materials and Methods* for details).

We collected the change in tumor volume and the mRECIST classification for a total of 3,127 experiments with reported treatment outcome, comprising 187 PDXs tested for response to 53 treatments. Figure 4B shows that TCT4U models are applicable to all drug-PDX pairs (3,127), while alterations in approved and experimental biomarkers can only be found in about half of them (1,758). However, wherever applicable, the accuracy attained by both methods is almost identical: TCT4U correctly classified 64% of sensitive and 56% of resistant drug-PDX pairs, while approved or experimental biomarkers attained sensitivity and resistance accuracies of 65% and 55%, respectively. Overall, TCT4U models yielded correct predictions for 1,866 (60%) drug-PDX pairs, while the figure achieved by known biomarkers is 1,048 (33%). It is also remarkable that, even if they consider a much lower number of genes, both MSK-IMPACT and FM derived models achieved comparable prediction accuracies (Figure 4B, Supplementary Figure S3).

In a treatment decision setting, we would not need to predict the effects of every possible drug on each patient, but only those drugs that might work best or, also importantly, those drugs that would not work. Thus, when we considered only the top-10 highest scoring sensitivity and resistance drugs for each of the 187 PDXs (i.e. high-confidence predictions), the precision of TCT4U significantly improved to 66% and 77%, respectively. We found very similar numbers for approved biomarkers (70% and 78%) although, in this case, they could only predict drug response in 210 of the drug-PDX pairs, spanning 59 PDXs (Figure 4D). Overall, we obtained a strong association between predicted and observed drug responses when analyzing all TCT4U models (OR 2.65, p-value $2.4 \cdot 10^{-40}$) that was even stronger when we focused on the high-confidence ones (OR 6.34, p-value $1.1 \cdot 10^{-56}$). In both cases, these associations are two-fold stronger than the ones achieved by approved and experimental biomarkers (p-value $1.3 \cdot 10^{-16}$). Finally, if we only focus on the drug with the highest probability of response per PDX (i.e. the most realistic scenario), TCT4U correctly predicted 56 effective drugs in 70 PDXs (80% accuracy) and 49 inefficacious drugs in 74

PDXs (66% accuracy), while the corresponding figures achieved by approved and experimental biomarkers are 16 out of 18 correct sensitive (89% accuracy) and 18 out of 23 resistance predictions (83% accuracy). Please, note that for the remaining PDXs (117 sensitive and 113 resistant), our top sensitivity and resistance predictions had no experimental data available and, thus, we cannot assess their accuracy.

Finally, while the coverage of approved or experimental biomarkers is mostly limited to BRAF/MEK inhibitors, PI3K/mTOR inhibitors or cell cycle related treatments, the predictions made by TCT4U also cover other drug families including chemotherapies, RTK inhibitors, endocrine therapies, and more experimental treatments targeting *WNT* (WNT974), *SHH* (LDE225) or apoptosis related pathways (TAS266, LGW813), among others (Figure 4E).

Experimental validation of TCT4U drug response predictions on a prospective PDX dataset

Additionally, we sought to prospectively evaluate the performance of the TCT4U models in new tumors. To this aim, we selected, from our VHIO collection of molecularly-characterized breast cancer PDXs, a subset of 15 tumors for which TCT4U prediction were of high confidence (i.e. in the top 10). Moreover, to assess the added value of our drug response predictors, we selected drug-PDX pairs for which the anticipated outcome did not agree with approved or experimental biomarkers, either because the individual oncogenomic profiles did not have any biomarker altered (n=9), or the TCT4U predictions were opposed to those suggested by known biomarkers (n=7). The final validation set consisted of 16 drug-PDX pairs, with 10 tumors predicted to be sensitive and 6 to be resistant, comprising an isoform-selective PI3Kα inhibitor (alpelisib, n=5), a CDK4/6 inhibitor (ribociclib, n=2), the combination of both (alpelisib+ribociclib, n=3), a MEK inhibitor (selumetinib, n=2), an estrogen receptor antagonist (tamoxifen, n=2), and a taxane (paclitaxel, n=2). We subcutaneously implanted the tumors in immunocompromised mice and let the tumors grow until they reached a volume of 120-150 mm^3. We then treated the PDXs for 15-57 days and measured their response to the administered drugs following the mRECIST guidelines (see Materials and Methods for details). The complete results of our study, including treatment setting (drug dose, duration, etc.) and tumor response (tumor growth, mRECIST classification, etc.) for every PDX can be found in Table S3, and are summarized in Figure 5.

We treated five PDXs with alpelisib, four of which (PDX131, PDX293, PDX156 and PDX191) were predicted to be sensitive to the drug by TCT4U models, and one (PDX153) to be resistant. The four PDXs predicted to be sensitive showed co-alterations of *CCND1*, *FGF3* and *FGF4*. These genes are located in the 11q13.3 genomic segment, and DCO networks found this region to be amplified more often in sensitive than in resistant PDXs, with an alteration rate of 7.46% and 1.37%, respectively (e-value 0.05). It is worth noting that our model, which was derived from 140 PDXs of different tumor types (i.e. 38 BRCA, 42 COADREAD, 25 NSCLC and 35 PDAC), did not show a significant tendency towards co-occurrence of PIK3CA and the 11q amplicon (OR 2.69 p-value 0.26).

Dysregulation of FGFR signaling can lead to downstream activation of PI3K/AKT pathway and, indeed, a recent study reported that 73% of patients (8 of 11) with both an alteration in the PI3K/AKT/mTOR pathway and FGF/FGFR amplification experienced clinical benefit when treated with therapy targeting the PI3K/AKT/mTOR pathway, whereas only 34% of patients (12 of 35) with PI3K/AKT/mTOR alterations alone did so [54]. However, the implication of FGF signaling with respect to the clinical benefit of PI3K/AKT/mTOR blockage remains controversial. The retrospective analysis of a large subset of patients enrolled in the BOLERO-2 trial [55] showed that alterations in FGF signaling had a negligible impact (*FGFR1*) or slightly decreased (*FGFR2*) the clinical benefit of everolimus treatment. In line with these findings, ER+/*ERBB2*- metastatic breast cancer patients with *FGFR1* and *FGFR2* amplification did not derive a clinical benefit from alpelisib+letrozole [56]. Accumulating evidence suggests that FGF signaling by FGFR1/2 amplification attenuates the response to PI3K blockage in PIK3CA mutant breast cancer. However, the impact of FGF signaling in response to alpelisib in PIK3CA wild-type tumors originated from breast as well as from other tissues has yet to be determined.

In our dataset, three out of the four PDXs responded to the treatment. In particular, in PDX293 we observed a partial response (PR) after 18 days of treatment, with a reduction of 65% in the initial tumor volume. PDX131 and PDX156 showed a stable disease (SD) after 20 and 11 days of treatment, respectively. On the other hand, in PDX191 the tumor increased its volume by 80% after 13 days of treatment (PD), and we thus considered it a wrong prediction. However, after 43 days of treatment, we could observe a halving in tumor growth (235%) with respect to untreated animals (501%) (Table S3). PDX153 was the only PDX with an oncogenic PIK3CA mutation (p.K111E) reported to confer sensitivity to the treatment [14] and, indeed, we observed a significant reduction of 83% in the tumor volume after 35 days of treatment (i.e. a PR outcome). Our model classified this PDX as resistant because it also had other alterations overrepresented among resistant PDXs, such as *MAP2K4* (e-value 0.011) or *NCOR1* (e-value 0.016). The DCO networks also considered *PIK3CA* status, which is more frequently altered in sensitive PDXs (22.29%) than in resistant PDXs (11.40%; e-value 0.071). However, it seems that the final prediction was driven by additional oncogenic alterations that showed stronger statistical association than *PIK3CA* status, although they proved to be less informative.

We administered ribociclib, a CDK4/6 inhibitor, to PDX4 and PDX244_LR1, with the TCT4U prediction that the two tumors would be resistant to the drug. PDX4 did not present any known biomarker of drug response, but it showed a heterozygous loss of *NF2*. Oncogenic alterations in *NF2* are overrepresented among resistant PDXs in the DCO network (e-value 0.037) and for this reason PDX4 was predicted to be resistant. Interestingly, loss of NF2 has been associated to increased CDK6 expression and was previously identified as mechanism of resistance to CDK4/6 inhibition in ER+ mestastatic breast cancer patients [57]. On the other hand, we also treated PDX244_LR1, which is a model of acquired resistance to ribociclib derived from a sensitive parental tumor (PDX244). Accordingly, PDX244_LR1 simultaneously showed known biomarkers of sensitivity (*CDKN2A-CDKN2B* co-deletion) and resistance (*TP53* p.C176R) to the treatment [14]. Although both genomic events were also considered by TCT4U models and, in line with what has been reported, *CDKN2A-CDKN2B* co-deletion is slightly more common in sensitive than in resistant PDXs

(32.78% vs. 25.34%; e-value 0.200), we did not find a significant association of *TP53* with resistance (44.65% vs. 48.39%; e-value 0.480), and thus it is not included in the ribociclib DCO network. Moreover, PDX244_LR1 presents an oncogenic mutation in *RB1* (p.M695Nfs*26), which showed a strong association with resistance to CDK4/6 inhibition in the DCO networks (4.29% vs. 12.65%, DiffD e-val 0.037). *RB1* is the primary target of CDK4/6 and its status is a key determinant of CDK4/6 inhibition efficacy [58]. Accordingly, *RB1* overexpression is reported to confer sensitivity to CDK4/6 inhibition in prostate cancer, but its loss or deletion is not currently reported as a resistance biomarker [14]. Our experiments showed that, and in agreement with TCT4U predictions, the tumors increased their volume between 45 and 215%, being thus catalogued as PD.

We also treated three PDXs (PDX173, PDX98 and PDX39) with the same PI3Kα and CDK4/6 inhibitors in combination (alpelisib+ribociclib). The three of them had oncogenic mutations in *TP53* (p.R249S, p.R249S and p.V157I), which are associated with resistance to CDK4/6 inhibition [14]. However, DCO networks found additional sensitivity-associated genomic features and thus TCT4U models predicted them as sensitive to this drug combination. More specifically, *TBX3* disrupting mutation, present in PDX173 and PDX98 DCO networks, is significantly associated to sensitivity to this treatment (6.19% vs. 0.05%; e-value 0.006). We found that, indeed, all three tumors responded to the combination treatment: PDX173 became completely tumor free (CR), PDX39 showed a reduction of 47% (SD), and PDX98 of 25% (SD). Interestingly, *TBX3* is a transcriptional repressor of p21 and p14, which are directly upstream of cyclin-CDKs, and also of *PTEN* [59]. *TBX3* has been shown to directly repress *PTEN* in neck squamous carcinoma cells [60], and thus *TBX3* loss would result in *PTEN* up-regulation influencing the response to PI3K inhibition. Although this hypothesis seems plausible, *TBX3* loss showed a low allelic fraction in PDX173 and its direct implication in response to this drug combination should be confirmed experimentally.

Two PDXs were treated with the MEK inhibitor Binimetinib, with TCT4U models predicting PDX270 to be resistant and PDX288 to respond to the drug. Both PDXs presented *RB1* loss (a loss-of-function mutation p.Y321* and a deletion, respectively), which is significantly associated to resistance in the DCO network (5.51% vs. 16.89%; e-value 0.015). Additional alterations necessarily contributed to the divergent prediction of those PDXs. The prediction of resistance in PDX270 was not likely to be driven by *TP53* loss, since DCO networks did not find this alteration significantly associated to MEK inhibition response (51.53% vs. 41.03%; e-value 0.165). The two PDXs also shared *MYC* amplification, which in our DCO networks is also not significantly associated to differential response to MEK inhibition (21.85% vs. 24.19%; e-value 0.730). However, we found that *MYC* was significantly co-altered with *SOX17* in PDX288. This co-alteration is distinctive of sensitive PDXs, with an observed co-occurrence rate of 13.11% with respect to an expected 3.09% (e-value $< 1 \cdot 10^{-4}$), and drove the TCT4U prediction. In this case, neither tumor presented known biomarkers of response to MEK inhibition. When treated with Binimetinib, PDX270 was classified as non-responder (PD), as the tumor volume had increased by 144%, even more than in untreated animals (117%). On the contrary, and validating the TCT4U models, PDX288 responded well to treatment (SD), and tumors did not show any significant growth. Interestingly, an integrative genomics screen performed in 229 primary invasive breast carcinomas identified the co-amplification of MYC and the 8p11-12 genomic region,

together with aberrant methylation and expression of several genes spanning the 8q12.1-q24.22 genomic region [61]. This observation coincides with our DCO network derived from whole exome sequencing data, where we could detect the co-amplification of a large cluster of genes located in the 8p11-p12 (*HOOK3*, *TCEA1*) and 8q11.23-q24.22 genomic regions (*SOX17*, *PLAG1*, *CHCHD7*, *NCOA2*, *COX6C*, *MYC*, *NDRG1*) in sensitive PDXs, but not in resistant ones (Supplementary Figure S1C-D).

We selected two additional PDXs to be treated with an estrogen receptor (*ER*) antagonist (tamoxifen) and, in agreement with TCT4U prediction,, we could confirm that both tumors were resistant to this treatment. PDX313 was ER+ but TCT4U models predicted it as resistant because it presents several alterations, namely *AKT1* p.E17K (0.08% vs. 8.75%, e-value 0.007), *NTRK1* amplification in chromosome 1 (0.20% vs. 23.29%, e-value 0.004), and the co-amplification of *CCND2-KDM5A* in chromosome 12 (0.06% vs. 23.15%, e-value 0.002; and 0.06% vs. 20.26%, e-value 0.002), that are associated to resistance in the DCO network. Moreover, this PDX had an oncogenic mutation in *NF1* (p.L375V) that, despite being associated to tamoxifen sensitivity in neuroblastoma [14, 62], has been associated to endocrine resistance in $HR^{+}HER2^{-}$ breast cancer patients [63].

Likewise, our models predicted resistance in STG201, an ER- PDX. It is noteworthy that the current implementation of TCT4U does not consider ER status because this biomarker cannot be determined from somatic DNA alterations. However, our method might still be able to detect subtype specific dependencies that might influence response to endocrine therapy. In tamoxifen DCO, the co-alteration of *CDKN2A-CDKN2B*, but not the alteration of *CDKN2A* alone (19.79% vs. 29.60%; e-value 0.515), is associated to resistance (17.89% vs. 5.30%, e-value 0.019) and is the genomic feature that more likely driving this prediction. Moreover, both tumors present oncogenic alterations in *TP53*, *CDKN2A-CDKN2B*, *CCND2* and *RB1* that might uncouple ER signaling and cell cycle progression (PDX313), which is a reported mechanism of resistance to endocrine therapy [64].

Finally, we explored the TCT4U prediction capacity in cytotoxic chemotherapy, where specific oncogenic characteristics should be less related to treatment efficacy. We selected PDX222 and PDX39 to be treated with Paclitaxel. While PDX222 did not present any known biomarker of response, PDX39 sowed an *MCL1* amplification, which has been reported to promote resistance to antitubulin chemotherapeutics [14, 65]. Although PDX222 showed alterations that are slightly more common in resistant than in sensitive PDXs (*EGFR*, *SOX17* and *APC*, all with insignificant e-values), it also presented an ERBB2 amplification that in our model is strongly associated to sensitivity (14.70% vs. 0.05%; e-value $6{\cdot}10^{-4}$), and a co-amplification of *FGFR4-NSD1* in chromosome 5, which also occurred more often than expected in sensitive than in resistant PDXs (7.33% vs. 0.54%, e-value 0.015). Regarding PDX39, the genomic feature with the strongest association in TCT4U was the same co-amplification of *FGFR4-NSD1* mentioned above, followed by the alteration of *GNAS* (7.49% vs. 2.81%; e-value 0.334), which is also slightly more frequent in sensitive than in resistant PDXs. Accordingly, we predicted that both tumors would respond to the drug. When treated with paclitaxel, both PDXs showed a progressive disease (PD), proving the TCT4U predictions wrong, although the growth of the tumors was 75% and 33% smaller in treated than in untreated mice.

Overall, TCT4U models correctly predicted the outcome of 12 of the 16 (75%) treatments tested, validating 70% of sensitivity (7 of 10) and 83% of resistance (5 of 6) predictions, which is in good agreement with the cross-validation results for high-confidence predictions (66-77% precision). However, in this challenging prospective validation, known biomarkers only predicted correctly 2 of the 16 (12%) treatment outcomes. In particular, two of the TCT4U misclassified responses were correctly predicted by known biomarkers, while the rest were either incorrect (5 of 7) or missing (9).

Bringing TCT4U from the workbench to the clinics

To explore the clinical potential of TCT4U methodology, we analyzed a cohort of 116 metastatic breast cancer patients being treated at the Memorial Sloan Kettering Cancer Center [57], and for which we have recorded information of their oncogenomic profile and clinical outcome (Table S4). These metastatic patients had received between 1 and 17 rounds of treatments (median of 2) before being selected for a trial to test a combination of CDK4/6 and aromatase inhibitors. Each tumor was genetically profiled, using the MSK-IMPACT panel, and the clinical outcome of the treatment was recorded as progression free survival (PFS). In this study, one third of the patients did not derive a clinical benefit and relapsed before 5 months. At the other extreme of the distribution, one third of the patients could be treated for more than 10 months and were considered to present a durable clinical benefit. We are aware that a threshold of 10 months might not be relevant in a first line treatment setting, where this drug combination has shown to achieve a median PFS of 24 months [66]. However, the PFS decreases in subsequent lines of therapy and, in a metastatic setting where over half of patients have received prior therapies, a PFS of more than 10 months might still be good surrogate measure of the clinical benefit.

We did not have PDXs treated with a combination of CDK4/6 and aromatase inhibitors, and the best TCT4U model for it was derived in response to CDK4/6 inhibition (ribociclib), based on 71 sensitive and 100 resistant PDXs. Using this model, only 6 out of 216 patients were predicted to be sensitive to treatment, and only one of them showed a clinically significant PFS (13.5 months). The majority of patients (78%) relapsed within the first year of treatment but, unfortunately, we have no data in this clinical series as to whether the tumors regressed, at least initially. It thus seems that the outcome measure used to train the TCT4U model (mRECIST), based on relative tumor growth, is not appropriate in most clinical settings.

Without a model for this specific drug combination, and with the aforementioned differences in outcome measures, we decided to adapt our methodology to classify patients based on the duration of the treatment before cancer relapsed. For this, we divided the cohort in three groups and considered the 40 patients for which the tumors relapsed before 4.2 months after the start of the treatment as resistant, and the 40 for which the time to progression was longer than 9.7 months as responsive to the treatment. The resulting DCO networks for this treatment, which are relatively small compared to TCT4U DCO networks, contain a total of 18 drivers and 16 co-occurring pairs (see Figure 6A). The

strongest associations captured by the DCO network are *MYC*, *MAP3K1*, *ATR* and *ERBB2* alterations, which happen more frequently in sensitive than in resistant patients (e-values of 0.001, 0.002, 0.004, and 0.033, respectively). On the other hand, we find that *MAP2K4*, *FGFR2*, *FAT1*, *ESR1* and *BCL6* are more frequently altered in resistant than in sensitive patients (e-values of 0.005, 0.005, 0.014, 0.017 and 0.044, respectively; Table S1). Indeed, *FAT1* loss has been recently associated to resistance to this treatment through a mechanism that involves the activation of Hippo pathway, leading to an increase in CDK6 expression [57]. Oncogenic mutations in *ESR1* are also common in metastatic and pretreated breast cancer, emerging as a mechanism of acquired resistance to endocrine therapies that can ultimately result in resistance to the combinational tehrapy [67].

Regarding driver co-occurrences, the triplet formed by *FGF3-FGF4-CCND1* oncogenes, located in the 11q13.3 genomic region, is co-altered more often in resistant than in sensitive patients. However, those three oncogenes tend to be co-altered with *PAK1* (in 11q14.1), more often in sensitive than in resistant patients (e-values of 0.006, 0.007 and 0.005). It has been suggested that the amplitude of the regions affected by copy number changes strongly determines patient prognosis [68]. Broader amplifications of this region (i.e spanning both 11q13 and 11q14) are likely to modify the dosage of multiple genes, which could have a cost in terms of cancer fitness and might contribute to the clinical benefit of the treatment.

On the other hand, *FGFR1* (8p11.23) alteration also tends to be co-altered with the four aforementioned genes (e-values of 0.008, 0.006, $6{\cdot}10^{-4}$ and 0.002) although this does not seem to affect drug response. It rather seems to reflect the putative synergy between the gain of function of *FGF3* and *FGF4* ligands and their cognate receptor *FGFR1*. Another interesting co-occurrence is *FGFR1-MDM2* co-alteration, which occurs more often than expected in resistant patients (e-value 0.020).

Overall, we saw that, although they shared a CDK4/6 inhibitor, the DCO networks were indeed very different to those derived in response to ribociclib, with only 3 of the 35 driver genes (*BCL6*, *FAT1*, and *MYC*) and none of the co-occurrences in common. We then used the DCO networks to derive the corresponding TCT4U models, which should be able to predict whether a given patient will obtain a significant clinical benefit.

In a leave-one-out cross validation, TCT4U models yielded confident scores for 78 out of the 116 patients (see *Materials and Methods*). Of these, we predicted that 43 patients would be sensitive and 35 resistant to the treatment. Indeed, we validated 19 of the 30 sensitive and 18 of the 27 resistant predictions (Figure 6), while the remaining 21 patients obtained an uncertain clinical benefit (i.e. TTP between 5 and 10 months). Put together, we obtained a significant association between the predicted and the observed clinical benefit (OR 3.45, p-value 0.022), with an overall accuracy of 67% (38 of 57).

Additionally, a Kaplan-Meier analysis of the cross-validation showed that the 35 patients predicted to relapse early, with a median time to progression of 4.2 months, derived little clinical benefit compared to the 43 patients predicted to relapse later, whose median time to progression was significantly longer (8.3 months, log-rank test p-value 0.030). We obtained consistent results when fitting a Cox proportional hazards regression model (correlation coefficient -0.37, p-value 0.022), indicating that TCT4U scores are correlated with progression free survival. The performance of TCT4U models clearly surpasses that of

known biomarkers for this drug combination. Although 56% (65 of 116) of patients had at least one annotated biomarker, which is a good coverage compared to other treatments, we could not find a significant association between observed and predicted outcomes, at least in terms of PFS (Figure 6).

Our results suggest that the proposed methodology could be used to derive DCO networks and train predictive models from the kind of data obtained from interim analyses in oncological clinical trials. Moreover, whenever the time to detect a clinical benefit is reasonable, such the 10 months in this study, TCT4U models could be derived with the first patients and used in population enrichment strategies to establish the bases for new recruitments in adaptive trials.

Concluding remarks

Cancer sequencing projects have unveiled hundreds of gene alterations driving tumorigenesis, enabling precision oncology. Indeed, current efforts now focus on the analyses of oncogenomic patterns to identify actionable alterations, drugs to modulate them and biomarkers to monitor response. Of particular interest are computational platforms such as OncoKB [13] or the Cancer Genome Interpreter [14], which not only identify oncogenic alterations and potential targets, but also estimate their potential clinical applicability. Most current strategies focus on the identification of a single vulnerability (i.e. driver gene) whose activity can be modulated by a drug. However, given the complexity and heterogeneity in tumors, and the high connectivity between cellular processes, every cancer might respond differently to a certain treatment, depending on its global oncogenomic profile.

Indeed, the analysis of the mutational landscape of cancer has also uncovered the existence of mutual exclusivity and co-occurrence patterns among driver gene alterations [16, 69]. Many computational tools have been developed to identify those combinatorial patterns experimentally (i.e via CRISPR-Cas9 screens [70, 71]) or computationally [72-79]. Patterns of mutual exclusivity can arise from functional redundancy, context-specific dependencies (i.e tumor type or sub-type specific driving alterations), or synthetic lethality interactions. While functional redundancy has been used to reveal unknown functional interactions [79], the synthetic lethality concept has been very successfully applied to the identification of novel therapeutic targets [70, 71] or rational drug combinations [71], and to the prediction of drug response in cell lines [71] and patients [78].

Although less studied, driver co-occurrences are often interpreted as a sign of synergy and in some cases they have shown to be functionally relevant [16-22]. However, they have not yet been exploited for drug response prediction. With the methodology presented in this manuscript, we compared the mutational profiles of tumors that are sensitive or resistant to a certain drug to define Driver Co-Occurrence (DCO) networks, which capture both genomic structure and putative oncogenic synergy. We then used the DCO networks to train classifiers to identify the best possible treatment for each tumor based on its oncogenomic profile.

The development of tools for personalized treatment prioritization based on genomic profiles is an active field of research. Recently Al-Shahrour and colleagues presented PanDrugs [80], an in silico drug prescription tool that uses genomic information, pathway context and pharmacological evidence to prioritize the drug therapies that are most suitable for individual tumor profiles. PanDrugs goes beyond the single-gene biomarker by taking into account the collective gene impact and pathway context of the oncogenic alterations identified in a given patient. However, it combines clinical evidence with *in vitro* drug screening data gathered from cancer cell line panels, which have limited clinical translatability [15, 27, 30, 81].

PANOPLY [82] is another computational framework that uses machine learning and knowledge-driven network analysis approaches to predict patient-specific drug response from multiomics profiles. This tool shows a great potential but the method strongly depends on whole genome and transcriptome patient data, which is not routinely acquired in clinical practice. Other methods like iCAGES [83] have been developed mainly to identify patient-specific driver genes from somatic mutation profiles, which are later used to prioritize drug treatments. However, iCAGES only considers drugs that directly target the identified driver alterations based on current FDA prescription guidelines. All those methods rely on prior knowledge, which is incomplete and biased, and have not been conceived to identify novel co-occurrence patterns from the data and to exploit them for drug response prediction.

With the current implementation of TCT4U, we present a collection of drug-response predictive models for 53 treatments belonging to 20 drug classes, including targeted and more conventional chemotherapies. In a cross-validation setting, our drug-response models attained a global accuracy similar to that of approved biomarkers, but could be applied to twice as many samples, including drug classes for which no biomarker is currently available. Moreover, in an *in vivo* prospective validation, our models correctly predicted 12 out of 16 responses to 6 drugs tested on 15 tumors.

Obviously, our approach also suffers from some limitations. Due to the lack of systematic reporting of treatment history of the patients enrolled in genomic studies [23], it is difficult to match response to a drug with individual molecular profiles from clinical data. This practically impairs the systematic assessment of the prediction accuracy in patients for computational frameworks like TCT4U, PanDrugs [80], PANOPLY [82], iCAGES [83], or other *in silico* drug prescription tools such as the Cancer Genome Interpreter [14] or OncoKB [13]. Experimental validation of computational approaches is time-intensive and very expensive. Therefore, beyond the thorough experimental validation presented in this manuscript, only PanDrugs and PANOPLY predictions were experimentally validated, although on a single case study performed on a PDX model that was treated with 5 drugs (PanDrugs) or 2 drugs (PANOPLY).

Given the limited clinical representativity of drug screens performed on cell lines [15, 27, 81], we relied on patient-derived xenografts (PDXs) to implement our strategy and to identify biomarkers of drug response. Although PDXs have shown a good level of agreement with the course of disease evolution and treatment response observed in the

tumors in the patient [30-33, 84, 85], they present some important drawbacks, such as the eventual loss of intratumoral heterogeneity [86, 87] or certain engraftment bias [30, 88]. Additionally, we have to consider that PDXs might not completely recapitulate the influence of the tissue of origin in tumors that have been implanted subcutaneously in immunodeficient mice and whose stroma has possibly regressed and/or been replaced by mouse stroma, altering thus their sub-clonal evolution and response to treatments [84, 89]. However, our strategy can be readily adapted to derive drug-response models from continuous clinical outcome measures, such as progression free survival, which better represent the data acquired during routine clinical practice and in clinical trials. Indeed, we derived response models on a clinical cohort of breast cancer metastatic patients being treated with a combination of CDK4/6 and aromatase inhibitors, showing a good correlation with progression free survival.

Most importantly, TCT4U drug-response DCO networks are interpretable, and provide clear hints to identify the potential mechanisms of sensitivity or resistance present in each tumor. However, one key challenge in interpreting driver alteration co-occurrence patterns is that they can also emerge without necessarily being synergistic if a pair of genes is affected by a common mutagenic process. This commonly happens when several oncogenes are co-amplified as part of the same genomic region and our method already accounts for this. However, co-occurrence patterns can also emerge as a result of the exposure to other mutagenic processes that increase the mutational burden, the chromosomal instability, or that leave specific mutational signatures [75, 76, 90]. Context or tumor type specific dependencies can also be a source of indirect associations with drug response. Although those confounding factors can obscure the biological interpretation of the DCO networks, they certainly provide valuable information for drug response prediction, especially in the case of ER status, which in most of the cases cannot be determined from somatic DNA alterations. Therefore, DCO networks are a valuable asset for hypothesis generation that need to be complemented with orthogonal sources of evidence, and functional validation will always be needed to demonstrate synergy. Indeed, we could find literature support for many of the candidate biomarkers identified, such as the loss of function of *FAT1* and *NF2* and their role in the development of resistance to CDK4/6 inhibitors [57] (Figure5, Figure6).

We also showed that our methodology is well suited to work with any custom gene panel, provided that the selected genes contribute to the differences in response to the drug being analyzed. As the cost of clinical molecular profiling continues to drop it is very likely that more types of data can be integratively analyzed to improve drug response prediction. However, in order to ensure the clinical translatability of our method in the short term, we decided to focus on well-supported oncogenic alterations that are readily detectable by cost effective methods in the clinical setting. We acknowledge that this is a very conservative decision and we accept that we might be missing biologically relevant information (i.e. non-coding alterations, methylation events or expression changes). Indeed, current clinical biomarkers for patient stratification are mostly based on the detection of histopathological, cytogenetic and immunohistochemical changes that are not always detectable at DNA sequence level. For example, breast cancer patient stratification strategies based on *ER*/*PR* and *ERBB2* status have proven to been very informative, both in terms of prognosis and response to treatment [91]. Accordingly, TCT4U predictions should

be regarded as a complementary source of information for clinical decision-making.

We believe that the computational framework presented, which goes beyond the single gene approach by exploiting co-occurrence patterns, could represent a significant advance towards the development of effective methods for personalized cancer treatment prioritization, with potential applications in population enrichment strategies in the context of adaptive clinical trials. Overall, our strategy represents an opportunity to accelerate the identification and validation of complex biomarkers with the potential to increase the impact of genomic profiling in precision oncology.

Materials and Methods

Genomic data processing

A total of 1,075 PDX models were established as part of a large pharmacogenomics screening that used the 'one animal per model per treatment' (1x1x1) experimental design to assess the population responses to 62 treatments [28]. We collected somatic mutations and copy number alterations for 375 of them, and used the *Cancer Genome Interpreter* resource [14] to classify protein-coding somatic mutations and copy number variants into predicted passenger or known/predicted oncogenic. In order to obtain comparable gene-wise oncogenic alteration rate estimates from a larger dataset of cancer patients, we downloaded the *Catalog of Driver Mutations (2016.5)*, a curated dataset of known and predicted oncogenic coding mutations identified after analyzing 6,792 exomes of a PanCancer cohort of 28 tumor types [7]. We complemented somatic driver mutations with copy number variation data for 4,058 patients representing 16 tumor types, accessed through cBioPortal [92]. We considered as oncogenic the deletion (GISTIC score ≤ -2) of tumor suppressor genes and the amplification (GISTIC score ≥ 2) of oncogenes. The role of driver genes was established by inspecting the Catalog of Cancer Genes [14]. In order to increase the clinical translatability, we subsampled both datasets to consider those oncogenic alterations covered by MSK-IMPACT [51] or by Foundation Medicine [53] targeted gene panels to obtain DCO networks and TCT4U models that could be directly used with those kind of molecular profiles, which are becoming widely used in the clinical setting.

Drug response data

In the original dataset, a total of 62 treatment groups were tested in 277 PDXs across six indications. Drug response was determined by analyzing the change in tumor volume with respect to the baseline along time. They combined two metrics (Best Response and Best Average Response) into a modified RECIST classification (mRECIST) with four classes: PD (progressive disease), SD (stable disease), PR (partial response) and CR (complete response). For our analyses, we considered PDXs whose tumors progressed upon treatment (PD) as resistant, and PDXs whose tumors stopped growing (SD) or regressed (PR, CR) as sensitive. After applying this binary classification, we had to exclude 9 treatments for which there were less than 5 PDXs in one of the two response groups, lacking thus enough interindividual heterogeneity to model drug response. A total of 276

PDXs were treated in at least one of the 53 treatment groups considered, each treatment being tested in 29 to 246 animals, with a median of 43 (IQR: 38-93). We could obtain the molecular profile for 187 of them, which had been treated with a median of 18 (IQR: 14-20) drugs. The final dataset consisted on 3,127 experiments performed on 187 PDXs and 53 treatment responses, across 5 tumor types: BRCA (breast cancer, n=38), CM (cutaneous melanoma, n=32), COREAD (colorectal carcinoma, n=51), NSCLC (non-small cell lung carcinoma, n=27), PAAD (pancreatic adenocarcinoma, n=38), and 1 PDX without tumor type annotation).

Molecular representativity of PDXs

We used the *OncoGenomic Landscapes* tool [35] to obtain a 2D representation of the molecular heterogeneity of the 187 PDXs being analyzed, and compared it to that of large reference cohorts of cancer patients. We downloaded the precomputed 2D projections of the following reference cohorts from the *OncoGenomic Landscapes* webserver (oglandscapes.irbbarcelona.org): PanCancer (n=15,212), BRCA (breast cancer, n=2,021), CM (cutaneous melanoma, n = 492), COREAD (colorectal carcinoma, n = 1,442), LUAD (lung adenocarcinoma, n = 1,486), LUSC (lung squamous cell carcinoma, n = 352), and PAAD (pancreatic adenocarcinoma, n = 442). We selected the 2D coordinates of the subset of TCGA and MSKCC patients of each reference cohort and represented their distribution in the PanCancer landscape as a level plot using the 2D kernel density estimate function of the 'seaborn' python library with 20 levels and a gray scale color-map as background. In order to highlight the territory occupied by the 187 PDXs, we obtained their 2D coordinates in the PanCancer landscape and generated a 2D kernel density estimate with the 'kdeplot' function using 10 levels, a transparent background, and contours colored using a color-map that represents probability density as heat.

Drug response prediction based on Cancer bioMarkers database

We manually mapped the set of 53 drugs and drug combinations tested in the cohort of PDXs to the corresponding drug families in the *Cancer bioMarkers database [14]* using drug target information available in ChEMBL and DrugBank (see Supplementary Table S4). We successfully assigned 50 out of the 53 treatments, spanning 29 drug family annotations. We considered those genomic alterations showing a 'complete match' with any of the reported predictive biomarkers and collapsed them at gene level. We considered as 'approved' biomarkers those ones that are currently approved by the FDA or by the main clinical guidelines in the field, such as the National Comprehensive Cancer Network (NCCN), the College of American Pathologists (CAP), the Clinical Pharmacogenetics Implementation Consortium (CPIC), or the European LeukemiaNet guidelines. We considered the rest of biomarkers, with varying supporting evidence, as 'experimental' biomarkers. The *Cancer bioMarkers database* usually reports more than one biomarker per drug or drug family, and often a single patient (or PDX) harbors several biomarkers of response and/or resistance for the same drug or drug family. We grouped response and resistance biomarkers at gene level and calculated the balanced accuracy (*BAcc*; average between sensitivity and specificity) of the prediction made by each gene in each treatment arm.

We weighted the binary predictions made by each gene and combined them to obtain a

final prediction per treatment and PDX ($wComb_{bmk}$).

Eq. 1:

$$wComb_{bmk} = \sum_{i \in S} BAcc_i \cdot s_i - \sum_{j \in R} BAcc_j \cdot s_j$$

S: Set of genes with or without predictive biomarkers of sensitivity (s_i, binary)
R: Set of genes with or without predictive biomarkers of resistance (s_j, binary)
$BAcc$: balanced accuracy of the predictive biomarker in a given treatment arm.

Driver Co-Occurrence (DCO) Networks

Differentially altered drivers (DiffD)

For each treatment, we aimed at identifying single gene biomarkers by selecting those driver genes with a significant differential alteration rate (DiffD) between sensitive and resistant PDXs. To this end, we compared the posterior probability distribution of the alteration rate of a given gene in sensitive versus resistant PDXs. We used a gene-specific informative prior based on the alteration rate observed in the cohort of 4,058 TCGA patients described above. In order to set a prior information contribution on the posterior inference to 5%, we set the effective population size of the prior to a 5% of the population size of the sample. These are the parameters of the beta posterior probability distribution of the alteration rate of a given gene in a given response group:

Eq. 2:

$$p(g_i|R) \sim Beta\left(k_R + \left(\frac{\alpha}{\alpha+\beta} \cdot \varepsilon \cdot n_R\right), n_R - k_R + \left(1 - \frac{\alpha}{\alpha+\beta} \cdot \varepsilon \cdot n_R\right)\right)$$

$p(g_i|R)$:oncogenic alteration probability of gene i in the response group R
k_R: number of PDXs in response group R with alterations in gene i
n_R: number of PDXs in response group R
α, β: number of patients in TCGA with and without oncogenic alterations in gene i, respectively
ε: constant representing the relative contribution of the prior to the posterior inference

We obtained an empirical distribution of DiffD by sampling 10,000 times the sensitive and resistant alteration rate posterior probability distributions and then obtained the probability that DiffD differs from 0 (DiffD e-value). We repeated this procedure considering the whole treatment arm and separately for each of the two response groups in order to identify three sets of genes per treatment arm: (i) sens_DiffD are those genes with more than 95% probability of showing higher alteration rate in the sensitive PDXs, (ii) res_DiffD are those genes with more than 95% probability of showing higher alteration rate in the resistant PDXs, and (iii) global_DiffD are those genes with more than 95% probability of showing differential alteration rate between the two response groups. Additionally, we required that

the selected genes were altered more than once in the corresponding group, with a minimum inferred alteration rate of 5%.

Driver Pairs (Ps)

To identify pairs of driver gene alterations occurring more often than expected in each response group of a given treatment arm, for each pair of co-altered drivers observed more than once in a given set of PDXs, we compared the observed probability of co-occurrence to the expected one under the independence assumption. To obtain the posterior probability distribution of the observed driver co-occurrence ($p(P_{ij}|R)$), we used a pair-specific informative prior based on the co-occurrence rate of this pair in the cohort of 4,058 TCGA patients, as described above. When this information was not available, we used a generic prior reflecting the average co-occurrence rate of any pair of drivers in TCGA. Again, we set a prior information contribution on the posterior inference to 5% by setting the effective population size of the prior to a 5% of the population size of the sample. These are the parameters of the beta posterior probability distribution of the co-occurrence rate of a given pair of gene alterations:

Eq. 3:

$$p(P_{ij}|R) \sim Beta\left(k_R + \left(\frac{\alpha}{\alpha+\beta}\cdot\varepsilon\cdot n_R\right), n_R - k_R + \left(1 - \frac{\alpha}{\alpha+\beta}\cdot\varepsilon\cdot n_R\right)\right)$$

$p(P_{ij}|R)$: alteration probability of gene i in the response group R
k_R: number of PDXs in response group R with co-alterations in genes i and j
n_R: number of PDXs in response group R
α, β: number of patients in TCGA with and without driver co-alterations in genes i and j, respectively
ε: constant representing the relative contribution of the prior to the posterior inference

To obtain the expected probability distribution of co-occurrence if genes g_i and g_j were independent, we sampled 10,000 times the posterior probability distribution of the alteration rate of each gene in the corresponding response group and computed their product ($p(g_i|R) \cdot p(g_j|R)$, see Eq. 2). We then obtained an empirical distribution of the difference between the observed and the expected co-occurrence rate ($p(P_{ji}|R) - p(g_i|R) \cdot p(g_j|R)$, see Eq. 3) and determined the probability that this difference was larger than 0 (Ps e-value). We repeated this procedure considering the whole treatment arm and separately for each of the two response groups in order to identify three sets of co-occurring drivers per treatment arm: (i) sens_Ps are those pairs of drivers with more than 95% probability of co-occurrence in the sensitive PDXs, (ii) res_Ps are those pairs of drivers with more than 95% probability of co-occurrence in the resistant PDXs, and (iii) global_Ps, which are those pairs of drivers with more than 95% probability of co-occurrence in the whole treatment arm. Additionally, we required that the selected pairs were altered more than once in the corresponding group, with a minimum inferred alteration rate of 5%. In the case of sens_Ps and res_Ps, we additionally required that the estimated co-occurrence rate was larger in the response group being considered than in the other one.

Driver Co-Occurrence (DCO) networks

The differentially-altered drivers (global_DiffD, sens_DiffD, res_DiffD) and pairs of co-altered drivers (global_Ps, sens_Ps and res_Ps) can be expressed in terms of co-occurrence networks, in which nodes representing differentially altered driver genes (DiffD) or driver genes involved in a pair of co-altered drivers (DiP) are connected according to significant co-occurrences (Ps). For each treatment arm, we obtained three of such networks: (i) a global network (global_DCO), (ii) a sensitivity network (sens_DCO), and (iii) a resistance network (res_DCO).

Genome adjacency clustering

We analyzed the topology of the DCO networks to characterize the genomic features of large densely connected modules (i.e Supplementary Figure S1C). We downloaded the genomic coordinates of human genes from UCSC genome browser to assess whether genomic linkage was influencing the probability of co-occurrence. For each DCO network, we computed the pairwise mutual information content between any pair of genes as follows.

Eq. 4:

$$MI(A,B) = \sum_{i=1}^{|A|}\sum_{j=1}^{|B|} P(i,j)\log\frac{P(i,j)}{P(i)P(j)}$$

$MI(A,B)$: Mutual Information content calculated for the pair of genes A and B
$P(i), P(j)$: probability that the status of gene A falls in class i in a PDX picked at random. Likewise for $P(j)$
$P(i,j)$: probability that the status of genes A and B fall in classes i and j in a PDX picked at random

We then represented the pairwise mutual information of all driver genes in the DCO network sorted by genomic coordinates and computed the Spearman's rank correlation between MI and physical distance in the genome for pairs of genes belonging to the same chromosome (i.e Supplementary Figure S2A). We applied an unsupervised clustering algorithm based on pairwise mutual information relative to genomic distance for pairs of drivers located in the same chromosome. More specifically, we retrieved a similarity graph from each DCO network after connecting every pair of driver genes located in the same chromosome by an edge weighted as follows.

Eq. 5:

$$AdjClust(A,B) = \begin{cases} \log\dfrac{MI(A,B)}{|TSS_a - TSS_b|} & chr_a = chr_b \\ NaN, & chr_a \neq chr_b \end{cases}$$

$AdjClust(A,B)$:adjacency clustering metric for the pair of genes A and B

TSS_g:chromosomal coordinates of the Transcriptional Start Site of gene g
chr_g:chromosome where gene g is located

Finally, we ran the MCL algorithm [93] with an *inflation* value of 2.5 and used the clusters with three or more driver genes for dimensionality reduction of the feature vectors describing the DCO networks.

Functional Analysis of the collection of DCO networks

We performed a functional analysis of the collection of DCO networks by calculating the enrichment of the 10 canonical cancer pathways identified and curated from the analysis of 9,125 samples from 33 cancer types [16]. The pathways analyzed are: cell cycle ('CellCycle'), Hippo signaling ('HIPPO'), Myc signaling ('MYC'), Notch signaling ('NOTCH'), oxidative stress response/Nrf2 ('NRF2'), PI-3-Kinase signaling ('PI3K'), receptor-tyrosine kinase (RTK)/RAS/MAP-Kinase signaling ('RTK-RAS'), TGFβ signaling ('TGF-Beta'), p53 ('TP53') and β-catenin/Wnt signaling ('WNT'). Those pathways capture key genes that are recurrently altered in cancer and are, therefore relatively small and specific, involving a total of 334 genes and 3 to 85 genes per pathway. We performed a Fisher's Exact test to assess whether the functions they represent were enriched or not among the set of biomarkers, the set of differentially altered drivers (DiffD), or the set of drivers in the DCO networks (DiffD_DiP) inferred for each treatment. We also checked whether each treatment was targeting a given pathway or not by mapping the drug target(s) of each treatment to the canonical cancer pathways. Finally, we performed a Fisher's exact test to assess whether the pathways that are enriched in each DCO network are also the pathways that are associated to the known mechanism of action of each treatment, in terms of drug targets.

TCT4U drug response classifiers

We described the DCO networks with a matrix of Boolean vectors (1: altered, 0: unaltered) encoding the alteration status of differentially altered drivers, drivers in co-occurring pairs, and pairs of drivers (DiffD_DiP_Ps) in each PDX. When needed, we adjusted for genomic linkage by reducing the dimensionality of the feature vectors and aggregating all drivers into clusters, which we considered to be altered when one or more of its constituent drivers were altered. We put together all those vectors in the form of a matrix and used it to train a Bernoulli Naïve Bayes (NB) classifier based on the observed responses to the treatment, also encoded as a Boolean vector (1: SD, PR, or CR; 0: PD). Please, note that we repeated the same procedure for each treatment arm with each of the three DCO networks described before (global_DiffD_DiP_Ps, sens_DiffD_DiP_Ps and res_DiffD_DiP_Ps). We assessed the accuracy and robustness of each of the three NB classifiers by performing an external leave-one-out cross validation (LOOCV) that involved both the inference of DCO networks and the prediction of drug response. We used the balanced accuracy of the LOOCV as weight to combine the global_DiffD_DiP_Ps, sens_DiffD_DiP_Ps and res_DiffD_DiP_Ps predictions generated for each drug-PDX pair into a final score, as described in Equation 5.

Eq. 6:

$$wComb = BAcc_{sNBC} \cdot I_{\{sNBC=1\}} \cdot P_s - BAcc_{rNBC} \cdot I_{\{rNBC=1\}} \cdot P_r + BAcc_{NBC} \cdot (I_{\{NBC=1\}} \cdot P_s - I_{\{NBC=0\}} \cdot P_r)$$

$sNBC$: binary prediction made by sens_DiffD_DiP_Ps NBC. A value of 1 indicates sensitivity
$rNBC$: binary prediction made by res_DiffD_DiP_Ps NBC. A value of 1 indicates resistance
NBC: binary prediction made by DiffD_DiP_Ps NBC. A value of 1 or 0 indicate sensitivity or resistance
P_s, P_r: Probability estimate for sensitivity or resistance, respectively.
$I_{\{NBC=j\}}$: Indicator function that takes a value of 1 when NBC predicts class j or a value of 0 otherwise.
$BAcc_{NBC}$: Balanced accuracy of the NBC in the LOOCV.

Experimental validation in PDXs

We collected all the available molecular profiles of the VHIO collection of breast cancer PDXs. Most PDXs were profiled using a hybridization-based capture panel of 410 genes (MSK-IMPACT) [51]. As we did for the training set, we used the Cancer Genome Interpreter resource [6] in order to filter out as many passenger alterations as possible. In the same way we did for the LOOCV, we described the molecular profile of each PDX according to the DiffD_DiP_Ps feature vectors associated to each DCO network and used them to predict the response to the 53 treatments in the TCT4U collection. For each PDX, we ranked all treatments based on the predicted response and focused on the 10 highest-scoring predictions of sensitivity and resistance. In order to increase the novelty of our findings, we excluded those predictions that were in agreement with predictions made by known predictive biomarkers. Then, we selected the 5 highest-scoring predictions of sensitivity and resistance per treatment. At this point, we had 51 novel, high-confidence predictions involving 32 PDXs and the following treatments: MEK inhibitor (n=15), Pi3K inhibitor (n=14), taxane (n=7), Pi3K inhibitor + CDK4/6 inhibitor (n=5), CDK4/6 inhibitor (n=5), and ER antagonist (n=5). We could recover raw experimental data for 10 drug-PDX pairs, including PDXs treated with Pi3K and/or CDK4/6, alone or in combination. We also found out that STG201 had already been reported to be resistant to tamoxifen (ER antagonist) (BCaPE REF). In order to cover the remaining treatment classes, we picked 6 additional drug-PDX pairs for experimental validation involving a MEK inhibitor (n=2), a taxane (n=2), and an ER antagonist (n=1). For each drug-PDX pair, 2 to 10 tumors were subcutaneously implanted in immunocompromised mice and grown until they reached a volume of 120-150 mm^3. Tumors were treated with either vehicle or the corresponding drug or combination at a clinically relevant dose. Tumor growth was measured at least twice per week for approximately 20 to 40 days, when typically tumor volume in the control group had doubled twice or more. Caliper measurements were converted into tumor volume estimates using the formula $(l \cdot w \cdot w) \cdot (\pi/6)$, where l and w are the major and minor tumor axes, respectively. The response was determined following the mRECIST guidelines that were used in the PDX screening that we used as training set [28]. Basically, we calculated the percentage change in tumor volume from baseline ($\Delta Vol_t = (V_t - V_i)/V_i \cdot 100$) and determined the BestResponse as the minimum value of ΔVol_t after 10 or more days of treatment. In order to capture tumor growth dynamics, we also calculated the

BestAverageResponse as the minimum value of $1/n \cdot \sum_{i=1}^{n} \Delta Vol_i$ after 10 or more days of treatment. PDXs were classified into response groups according to the mRECIST criteria applied in the following order:

CR: BestResp < -95% *and* BestAvgResp < -40%
PR: BestResp < -50% *and* BestAvgResp < -20%
SD: BestResp < 35% *and* BestAvgResp < 30%
PD: BestResp ≥ 35% *and* BestAvgResp ≥ 30%

Adaptation of TCT4U to use continuous clinical outcome measurements

We obtained both genomic and clinical data for a total of 116 patients with HR+/HER2- metastatic breast cancer that were treated with a CDK4/6 inhibitor in combination with an Aromatase Inhibitor in metastatic setting [57]. All patients underwent prospective clinical genomic profiling consisting on the identification of single nucleotide variants, small indels and copy number alterations detected from matched tumor-normal sequence data using the MSK-IMPACT targeted gene panels. We used the Cancer Genome Interpreter [14] to filter out passenger mutations and CNVs. and keep only known or predicted driver mutations or copy number alterations. Detailed treatment history data was collected for each patient and included all lines of systemic therapy from the time of diagnosis of invasive carcinoma to the study data lock in September 2017. The exact regimen, as well as the dates of start and stop of therapy were also recorded. For the current analysis, we considered the treatment duration time as a measure of clinical benefit derived by patients whose biopsies were collected prior to or within the first 60 days of therapy initiation.

We used the TCT4U model of response to ribociclib to predicted response to CDK4/6 inhibition, as described before. Due to the differences in clinical outcome measurements between the training and the clinical cohort, we decided to adapt the TCT4U methodology to use continuous clinical outcome measurements as training set, instead of binary classification of drug response based on tumor growth. Our strategy consisted on comparing extreme populations both to derive the DCO networks and to train the classifier. We partitioned the population into three equally sized sets and applied the methodology described above. In this exercise, we set the cut-offs at 4.2 months and 9.7 months. We selected as sens_DiffD or res_DiffD those genes with more than 95% probability of showing higher alteration rate in the one third of patients showing the most durable or shortest clinical benefit, respectively, compared to the third of patients at the other extreme of the distribution. Additionally, we selected as global_DiffD all those genes with more than 95% probability of showing differential alteration rate between the two extreme populations. The same strategy was applied in the identification of pairs of driver gene alterations occurring more often than expected considering all patients (global_Ps) or separately for the one third of patients that relapsed the latest (sens_Ps) or the earliest (res_Ps). The remaining steps were applied exactly as described for the binary TCT4U methodology. In this setting with only one treatment per patient, high confidence predictions were selected by optimizing the threshold of the global score to get a maximum false discovery rate of 30% in the LOOCV.

Acknowledgments

The authors would like to thank IRB Barcelona and VHIO colleagues for providing feedback on the work, and Dr David Torrents (ICREA-BSC) for critically reading the manuscript. V.S. thanks Faye Su (Novartis Oncology) for providing study reagents alpelisib (BYL719) and ribociclib (LEE011).

Grant Support

L.M. is a recipient of an FPI fellowship. P.A. acknowledges the support of the Spanish Ministerio de Economía y Competitividad (BIO2016-77038-R) and the European Research Council (SysPharmAD: 614944). V.S. is recipient of a Miguel Servet grant from ISCIII (CP14/00228) and receives funds from AGAUR (2017 SGR 540). The PDX program is supported by a GHD-Pink (FERO foundation) grant to V.S.. A.G.-O. and M.P. received a FI-AGAUR and a Juan de la Cierva (MJCI-2015-25412) fellowship, respectively.

Conflicts of Interest

PR reports consulting/advisory board for Novartis and institutional research support from Illumina and GRAIL, Inc.

References

1. Stockley TL, Oza AM, Berman HK, Leighl NB, Knox JJ, Shepherd FA, Chen EX, Krzyzanowska MK, Dhani N, Joshua AM *et al*: **Molecular profiling of advanced solid tumors and patient outcomes with genotype-matched clinical trials: the Princess Margaret IMPACT/COMPACT trial**. *Genome Med* 2016, **8**(1):109.
2. Schwaederle M, Zhao M, Lee JJ, Eggermont AM, Schilsky RL, Mendelsohn J, Lazar V, Kurzrock R: **Impact of Precision Medicine in Diverse Cancers: A Meta-Analysis of Phase II Clinical Trials**. *J Clin Oncol* 2015, **33**(32):3817-3825.
3. Jardim DL, Schwaederle M, Wei C, Lee JJ, Hong DS, Eggermont AM, Schilsky RL, Mendelsohn J, Lazar V, Kurzrock R: **Impact of a Biomarker-Based Strategy on Oncology Drug Development: A Meta-analysis of Clinical Trials Leading to FDA Approval**. *J Natl Cancer Inst* 2015, **107**(11).
4. Prasad V: **Perspective: The precision-oncology illusion**. *Nature* 2016, **537**(7619):S63.
5. Chang MT, Bhattarai TS, Schram AM, Bielski CM, Donoghue MTA, Jonsson P, Chakravarty D, Phillips S, Kandoth C, Penson A *et al*: **Accelerating Discovery of Functional Mutant Alleles in Cancer**. *Cancer Discov* 2018, **8**(2):174-183.
6. Bailey MH, Tokheim C, Porta-Pardo E, Sengupta S, Bertrand D, Weerasinghe A, Colaprico A, Wendl MC, Kim J, Reardon B *et al*: **Comprehensive Characterization of Cancer Driver Genes and Mutations**. *Cell* 2018, **173**(2):371-385 e318.
7. Rubio-Perez C, Tamborero D, Schroeder MP, Antolin AA, Deu-Pons J, Perez-Llamas C, Mestres J, Gonzalez-Perez A, Lopez-Bigas N: **In silico prescription of anticancer drugs to cohorts of 28 tumor types reveals targeting opportunities**. *Cancer Cell* 2015, **27**(3):382-396.
8. Senft D, Leiserson MDM, Ruppin E, Ronai ZA: **Precision Oncology: The Road Ahead**. *Trends Mol Med* 2017, **23**(10):874-898.
9. Das S, Lo AW: **Re-inventing drug development: A case study of the I-SPY 2 breast cancer clinical trials program**. *Contemp Clin Trials* 2017, **62**:168-174.
10. Simon R: **Critical Review of Umbrella, Basket, and Platform Designs for Oncology Clinical Trials**. *Clin Pharmacol Ther* 2017, **102**(6):934-941.

11. Pallmann P, Bedding AW, Choodari-Oskooei B, Dimairo M, Flight L, Hampson LV, Holmes J, Mander AP, Odondi L, Sydes MR *et al*: **Adaptive designs in clinical trials: why use them, and how to run and report them**. *BMC Med* 2018, **16**(1):29.
12. Thorlund K, Haggstrom J, Park JJ, Mills EJ: **Key design considerations for adaptive clinical trials: a primer for clinicians**. *BMJ* 2018, **360**:k698.
13. Chakravarty D, Gao J, Phillips SM, Kundra R, Zhang H, Wang J, Rudolph JE, Yaeger R, Soumerai T, Nissan MH *et al*: **OncoKB: A Precision Oncology Knowledge Base**. *JCO Precis Oncol* 2017, **2017**.
14. Tamborero D, Rubio-Perez C, Deu-Pons J, Schroeder MP, Vivancos A, Rovira A, Tusquets I, Albanell J, Rodon J, Tabernero J *et al*: **Cancer Genome Interpreter annotates the biological and clinical relevance of tumor alterations**. *Genome Med* 2018, **10**(1):25.
15. Jaeger S, Duran-Frigola M, Aloy P: **Drug sensitivity in cancer cell lines is not tissue-specific**. *Mol Cancer* 2015, **14**:40.
16. Sanchez-Vega F, Mina M, Armenia J, Chatila WK, Luna A, La KC, Dimitriadoy S, Liu DL, Kantheti HS, Saghafinia S *et al*: **Oncogenic Signaling Pathways in The Cancer Genome Atlas**. *Cell* 2018, **173**(2):321-337 e310.
17. Huun J, Lonning PE, Knappskog S: **Effects of concomitant inactivation of p53 and pRb on response to doxorubicin treatment in breast cancer cell lines**. *Cell Death Discov* 2017, **3**:17026.
18. Tu Q, Hao J, Zhou X, Yan L, Dai H, Sun B, Yang D, An S, Lv L, Jiao B *et al*: **CDKN2B deletion is essential for pancreatic cancer development instead of unmeaningful co-deletion due to juxtaposition to CDKN2A**. *Oncogene* 2018, **37**(1):128-138.
19. Dembla V, Somaiah N, Barata P, Hess K, Fu S, Janku F, Karp DD, Naing A, Piha-Paul SA, Subbiah V *et al*: **Prevalence of MDM2 amplification and coalterations in 523 advanced cancer patients in the MD Anderson phase 1 clinic**. *Oncotarget* 2018, **9**(69):33232-33243.
20. Laroche-Clary A, Chaire V, Algeo MP, Derieppe MA, Loarer FL, Italiano A: **Combined targeting of MDM2 and CDK4 is synergistic in dedifferentiated liposarcomas**. *J Hematol Oncol* 2017, **10**(1):123.
21. Lauber C, Klink B, Seifert M: **Comparative analysis of histologically classified oligodendrogliomas reveals characteristic molecular differences between subgroups**. *BMC Cancer* 2018, **18**(1):399.
22. Ulz P, Heitzer E, Speicher MR: **Co-occurrence of MYC amplification and TP53 mutations in human cancer**. *Nat Genet* 2016, **48**(2):104-106.
23. Liu J, Lichtenberg T, Hoadley KA, Poisson LM, Lazar AJ, Cherniack AD, Kovatich AJ, Benz CC, Levine DA, Lee AV *et al*: **An Integrated TCGA Pan-Cancer Clinical Data Resource to Drive High-Quality Survival Outcome Analytics**. *Cell* 2018, **173**(2):400-416 e411.
24. Consortium APG: **AACR Project GENIE: Powering Precision Medicine through an International Consortium**. *Cancer Discov* 2017, **7**(8):818-831.
25. Guinney J, Saez-Rodriguez J: **Alternative models for sharing confidential biomedical data**. *Nat Biotechnol* 2018, **36**(5):391-392.
26. Iorio F, Knijnenburg TA, Vis DJ, Bignell GR, Menden MP, Schubert M, Aben N, Goncalves E, Barthorpe S, Lightfoot H *et al*: **A Landscape of Pharmacogenomic Interactions in Cancer**. *Cell* 2016, **166**(3):740-754.
27. Gillet JP, Varma S, Gottesman MM: **The clinical relevance of cancer cell lines**. *J Natl Cancer Inst* 2013, **105**(7):452-458.
28. Gao H, Korn JM, Ferretti S, Monahan JE, Wang Y, Singh M, Zhang C, Schnell C, Yang G, Zhang Y *et al*: **High-throughput screening using patient-derived tumor xenografts to predict clinical trial drug response**. *Nat Med* 2015, **21**(11):1318-1325.
29. Einarsdottir BO, Bagge RO, Bhadury J, Jespersen H, Mattsson J, Nilsson LM, Truve K, Lopez MD, Naredi P, Nilsson O *et al*: **Melanoma patient-derived xenografts accurately model the disease and develop fast enough to guide treatment decisions**. *Oncotarget* 2014, **5**(20):9609-9618.
30. Bruna A, Rueda OM, Greenwood W, Batra AS, Callari M, Batra RN, Pogrebniak K, Sandoval J, Cassidy JW, Tufegdzic-Vidakovic A *et al*: **A Biobank of Breast Cancer Explants with Preserved Intra-tumor Heterogeneity to Screen Anticancer Compounds**. *Cell* 2016, **167**(1):260-274 e222.
31. Krepler C, Sproesser K, Brafford P, Beqiri M, Garman B, Xiao M, Shannan B, Watters A,

Perego M, Zhang G *et al*: **A Comprehensive Patient-Derived Xenograft Collection Representing the Heterogeneity of Melanoma**. *Cell Rep* 2017, **21**(7):1953-1967.

32. Pompili L, Porru M, Caruso C, Biroccio A, Leonetti C: **Patient-derived xenografts: a relevant preclinical model for drug development**. *J Exp Clin Cancer Res* 2016, **35**(1):189.
33. Byrne AT, Alferez DG, Amant F, Annibali D, Arribas J, Biankin AV, Bruna A, Budinska E, Caldas C, Chang DK *et al*: **Interrogating open issues in cancer precision medicine with patient-derived xenografts**. *Nat Rev Cancer* 2017, **17**(4):254-268.
34. Therasse P, Arbuck SG, Eisenhauer EA, Wanders J, Kaplan RS, Rubinstein L, Verweij J, Van Glabbeke M, van Oosterom AT, Christian MC *et al*: **New guidelines to evaluate the response to treatment in solid tumors. European Organization for Research and Treatment of Cancer, National Cancer Institute of the United States, National Cancer Institute of Canada**. *J Natl Cancer Inst* 2000, **92**(3):205-216.
35. Mateo L, Guitart-Pla O, Duran-Frigola M, Aloy P: **Exploring the OncoGenomic Landscape of cancer**. *Genome Med* 2018, **10**(1):61.
36. Shannon P, Markiel A, Ozier O, Baliga NS, Wang JT, Ramage D, Amin N, Schwikowski B, Ideker T: **Cytoscape: a software environment for integrated models of biomolecular interaction networks**. *Genome Res* 2003, **13**(11):2498-2504.
37. Haarberg HE, Smalley KS: **Resistance to Raf inhibition in cancer**. *Drug Discov Today Technol* 2014, **11**:27-32.
38. McGlynn LM, Kirkegaard T, Edwards J, Tovey S, Cameron D, Twelves C, Bartlett JM, Cooke TG: **Ras/Raf-1/MAPK pathway mediates response to tamoxifen but not chemotherapy in breast cancer patients**. *Clin Cancer Res* 2009, **15**(4):1487-1495.
39. Arriola E, Marchio C, Tan DS, Drury SC, Lambros MB, Natrajan R, Rodriguez-Pinilla SM, Mackay A, Tamber N, Fenwick K *et al*: **Genomic analysis of the HER2/TOP2A amplicon in breast cancer and breast cancer cell lines**. *Lab Invest* 2008, **88**(5):491-503.
40. Gennari A, Sormani MP, Pronzato P, Puntoni M, Colozza M, Pfeffer U, Bruzzi P: **HER2 status and efficacy of adjuvant anthracyclines in early breast cancer: a pooled analysis of randomized trials**. *J Natl Cancer Inst* 2008, **100**(1):14-20.
41. Baselga J, Manikhas A, Cortes J, Llombart A, Roman L, Semiglazov VF, Byakhov M, Lokanatha D, Forenza S, Goldfarb RH *et al*: **Phase III trial of nonpegylated liposomal doxorubicin in combination with trastuzumab and paclitaxel in HER2-positive metastatic breast cancer**. *Ann Oncol* 2014, **25**(3):592-598.
42. Gao J, Aksoy BA, Dogrusoz U, Dresdner G, Gross B, Sumer SO, Sun Y, Jacobsen A, Sinha R, Larsson E *et al*: **Integrative analysis of complex cancer genomics and clinical profiles using the cBioPortal**. *Sci Signal* 2013, **6**(269):pl1.
43. Patnaik A, Rosen LS, Tolaney SM, Tolcher AW, Goldman JW, Gandhi L, Papadopoulos KP, Beeram M, Rasco DW, Hilton JF *et al*: **Efficacy and Safety of Abemaciclib, an Inhibitor of CDK4 and CDK6, for Patients with Breast Cancer, Non-Small Cell Lung Cancer, and Other Solid Tumors**. *Cancer Discov* 2016, **6**(7):740-753.
44. Knudsen ES, Witkiewicz AK: **The Strange Case of CDK4/6 Inhibitors: Mechanisms, Resistance, and Combination Strategies**. *Trends Cancer* 2017, **3**(1):39-55.
45. Sweeney KJ, Sarcevic B, Sutherland RL, Musgrove EA: **Cyclin D2 activates Cdk2 in preference to Cdk4 in human breast epithelial cells**. *Oncogene* 1997, **14**(11):1329-1340.
46. Juric D, Janku F, Rodon J, Burris HA, Mayer IA, Schuler M, Seggewiss-Bernhardt R, Gil-Martin M, Middleton MR, Baselga J *et al*: **Alpelisib Plus Fulvestrant in PIK3CA-Altered and PIK3CA-Wild-Type Estrogen Receptor-Positive Advanced Breast Cancer: A Phase 1b Clinical Trial**. *JAMA Oncol* 2019, **5**(2):e184475.
47. Juric D, Rodon J, Tabernero J, Janku F, Burris HA, Schellens JHM, Middleton MR, Berlin J, Schuler M, Gil-Martin M *et al*: **Phosphatidylinositol 3-Kinase alpha-Selective Inhibition With Alpelisib (BYL719) in PIK3CA-Altered Solid Tumors: Results From the First-in-Human Study**. *J Clin Oncol* 2018, **36**(13):1291-1299.
48. Andre F, Ciruelos E, Rubovszky G, Campone M, Loibl S, Rugo HS, Iwata H, Conte P, Mayer IA, Kaufman B *et al*: **Alpelisib for PIK3CA-Mutated, Hormone Receptor-Positive Advanced Breast Cancer**. *N Engl J Med* 2019, **380**(20):1929-1940.
49. Nakanishi Y, Walter K, Spoerke JM, O'Brien C, Huw LY, Hampton GM, Lackner MR: **Activating Mutations in PIK3CB Confer Resistance to PI3K Inhibition and Define a Novel Oncogenic Role for p110beta**. *Cancer Res* 2016, **76**(5):1193-1203.

50. Juric D, Castel P, Griffith M, Griffith OL, Won HH, Ellis H, Ebbesen SH, Ainscough BJ, Ramu A, Iyer G *et al*: **Convergent loss of PTEN leads to clinical resistance to a PI(3)Kalpha inhibitor**. *Nature* 2015, **518**(7538):240-244.
51. Cheng DT, Mitchell TN, Zehir A, Shah RH, Benayed R, Syed A, Chandramohan R, Liu ZY, Won HH, Scott SN *et al*: **Memorial Sloan Kettering-Integrated Mutation Profiling of Actionable Cancer Targets (MSK-IMPACT): A Hybridization Capture-Based Next-Generation Sequencing Clinical Assay for Solid Tumor Molecular Oncology**. *J Mol Diagn* 2015, **17**(3):251-264.
52. Zehir A, Benayed R, Shah RH, Syed A, Middha S, Kim HR, Srinivasan P, Gao J, Chakravarty D, Devlin SM *et al*: **Mutational landscape of metastatic cancer revealed from prospective clinical sequencing of 10,000 patients**. *Nat Med* 2017, **23**(6):703-713.
53. Frampton GM, Fichtenholtz A, Otto GA, Wang K, Downing SR, He J, Schnall-Levin M, White J, Sanford EM, An P *et al*: **Development and validation of a clinical cancer genomic profiling test based on massively parallel DNA sequencing**. *Nat Biotechnol* 2013, **31**(11):1023-1031.
54. Wheler JJ, Atkins JT, Janku F, Moulder SL, Stephens PJ, Yelensky R, Valero V, Miller V, Kurzrock R, Meric-Bernstam F: **Presence of both alterations in FGFR/FGF and PI3K/AKT/mTOR confer improved outcomes for patients with metastatic breast cancer treated with PI3K/AKT/mTOR inhibitors**. *Oncoscience* 2016, **3**(5-6):164-172.
55. Hortobagyi GN, Chen D, Piccart M, Rugo HS, Burris HA, 3rd, Pritchard KI, Campone M, Noguchi S, Perez AT, Deleu I *et al*: **Correlative Analysis of Genetic Alterations and Everolimus Benefit in Hormone Receptor-Positive, Human Epidermal Growth Factor Receptor 2-Negative Advanced Breast Cancer: Results From BOLERO-2**. *J Clin Oncol* 2016, **34**(5):419-426.
56. Mayer IA, Abramson VG, Formisano L, Balko JM, Estrada MV, Sanders ME, Juric D, Solit D, Berger MF, Won HH *et al*: **A Phase Ib Study of Alpelisib (BYL719), a PI3Kalpha-Specific Inhibitor, with Letrozole in ER+/HER2- Metastatic Breast Cancer**. *Clin Cancer Res* 2017, **23**(1):26-34.
57. Li Z, Razavi P, Li Q, Toy W, Liu B, Ping C, Hsieh W, Sanchez-Vega F, Brown DN, Da Cruz Paula AF *et al*: **Loss of the FAT1 Tumor Suppressor Promotes Resistance to CDK4/6 Inhibitors via the Hippo Pathway**. *Cancer Cell* 2018, **34**(6):893-905 e898.
58. Shapiro GI: **Genomic Biomarkers Predicting Response to Selective CDK4/6 Inhibition: Progress in an Elusive Search**. *Cancer Cell* 2017, **32**(6):721-723.
59. Willmer T, Peres J, Mowla S, Abrahams A, Prince S: **The T-Box factor TBX3 is important in S-phase and is regulated by c-Myc and cyclin A-CDK2**. *Cell Cycle* 2015, **14**(19):3173-3183.
60. Burgucu D, Guney K, Sahinturk D, Ozbudak IH, Ozel D, Ozbilim G, Yavuzer U: **Tbx3 represses PTEN and is over-expressed in head and neck squamous cell carcinoma**. *BMC Cancer* 2012, **12**:481.
61. Parris TZ, Kovacs A, Hajizadeh S, Nemes S, Semaan M, Levin M, Karlsson P, Helou K: **Frequent MYC coamplification and DNA hypomethylation of multiple genes on 8q in 8p11-p12-amplified breast carcinomas**. *Oncogenesis* 2014, **3**:e95.
62. Byer SJ, Eckert JM, Brossier NM, Clodfelder-Miller BJ, Turk AN, Carroll AJ, Kappes JC, Zinn KR, Prasain JK, Carroll SL: **Tamoxifen inhibits malignant peripheral nerve sheath tumor growth in an estrogen receptor-independent manner**. *Neuro Oncol* 2011, **13**(1):28-41.
63. Razavi P, Chang MT, Xu G, Bandlamudi C, Ross DS, Vasan N, Cai Y, Bielski CM, Donoghue MTA, Jonsson P *et al*: **The Genomic Landscape of Endocrine-Resistant Advanced Breast Cancers**. *Cancer Cell* 2018, **34**(3):427-438 e426.
64. Thangavel C, Dean JL, Ertel A, Knudsen KE, Aldaz CM, Witkiewicz AK, Clarke R, Knudsen ES: **Therapeutically activating RB: reestablishing cell cycle control in endocrine therapy-resistant breast cancer**. *Endocr Relat Cancer* 2011, **18**(3):333-345.
65. Wertz IE, Kusam S, Lam C, Okamoto T, Sandoval W, Anderson DJ, Helgason E, Ernst JA, Eby M, Liu J *et al*: **Sensitivity to antitubulin chemotherapeutics is regulated by MCL1 and FBW7**. *Nature* 2011, **471**(7336):110-114.
66. Tanguy ML, Cabel L, Berger F, Pierga JY, Savignoni A, Bidard FC: **Cdk4/6 inhibitors and overall survival: power of first-line trials in metastatic breast cancer**. *NPJ Breast Cancer* 2018, **4**:14.

67. Preusser M, De Mattos-Arruda L, Thill M, Criscitiello C, Bartsch R, Ruhstaller T, de Azambuja E, Zielinski CC: **CDK4/6 inhibitors in the treatment of patients with breast cancer: summary of a multidisciplinary round-table discussion**. *ESMO Open* 2018, **3**(5):e000368.
68. Smith JC, Sheltzer JM: **Systematic identification of mutations and copy number alterations associated with cancer patient prognosis**. *Elife* 2018, **7**.
69. Kandoth C, McLellan MD, Vandin F, Ye K, Niu B, Lu C, Xie M, Zhang Q, McMichael JF, Wyczalkowski MA *et al*: **Mutational landscape and significance across 12 major cancer types**. *Nature* 2013, **502**(7471):333-339.
70. Behan FM, Iorio F, Picco G, Goncalves E, Beaver CM, Migliardi G, Santos R, Rao Y, Sassi F, Pinnelli M *et al*: **Prioritization of cancer therapeutic targets using CRISPR-Cas9 screens**. *Nature* 2019, **568**(7753):511-516.
71. Szlachta K, Kuscu C, Tufan T, Adair SJ, Shang S, Michaels AD, Mullen MG, Fischer NL, Yang J, Liu L *et al*: **CRISPR knockout screening identifies combinatorial drug targets in pancreatic cancer and models cellular drug response**. *Nat Commun* 2018, **9**(1):4275.
72. Wu H, Gao L, Li F, Song F, Yang X, Kasabov N: **Identifying overlapping mutated driver pathways by constructing gene networks in cancer**. *BMC Bioinformatics* 2015, **16 Suppl 5**:S3.
73. Szczurek E, Beerenwinkel N: **Modeling mutual exclusivity of cancer mutations**. *PLoS Comput Biol* 2014, **10**(3):e1003503.
74. Kim YA, Madan S, Przytycka TM: **WeSME: uncovering mutual exclusivity of cancer drivers and beyond**. *Bioinformatics* 2017, **33**(6):814-821.
75. Dao P, Kim YA, Wojtowicz D, Madan S, Sharan R, Przytycka TM: **BeWith: A Between-Within method to discover relationships between cancer modules via integrated analysis of mutual exclusivity, co-occurrence and functional interactions**. *PLoS Comput Biol* 2017, **13**(10):e1005695.
76. Canisius S, Martens JW, Wessels LF: **A novel independence test for somatic alterations in cancer shows that biology drives mutual exclusivity but chance explains most co-occurrence**. *Genome Biol* 2016, **17**(1):261.
77. Mina M, Raynaud F, Tavernari D, Battistello E, Sungalee S, Saghafinia S, Laessle T, Sanchez-Vega F, Schultz N, Oricchio E *et al*: **Conditional Selection of Genomic Alterations Dictates Cancer Evolution and Oncogenic Dependencies**. *Cancer Cell* 2017, **32**(2):155-168 e156.
78. Lee JS, Das A, Jerby-Arnon L, Arafeh R, Auslander N, Davidson M, McGarry L, James D, Amzallag A, Park SG *et al*: **Harnessing synthetic lethality to predict the response to cancer treatment**. *Nat Commun* 2018, **9**(1):2546.
79. Vandin F, Upfal E, Raphael BJ: **De novo discovery of mutated driver pathways in cancer**. *Genome Res* 2012, **22**(2):375-385.
80. Pineiro-Yanez E, Reboiro-Jato M, Gomez-Lopez G, Perales-Paton J, Troule K, Rodriguez JM, Tejero H, Shimamura T, Lopez-Casas PP, Carretero J *et al*: **PanDrugs: a novel method to prioritize anticancer drug treatments according to individual genomic data**. *Genome Med* 2018, **10**(1):41.
81. Domcke S, Sinha R, Levine DA, Sander C, Schultz N: **Evaluating cell lines as tumour models by comparison of genomic profiles**. *Nat Commun* 2013, **4**:2126.
82. Kalari KR, Sinnwell JP, Thompson KJ, Tang X, Carlson EE, Yu J, Vedell PT, Ingle JN, Weinshilboum RM, Boughey JC *et al*: **PANOPLY: Omics-Guided Drug Prioritization Method Tailored to an Individual Patient**. *JCO Clin Cancer Inform* 2018, **2**:1-11.
83. Dong C, Guo Y, Yang H, He Z, Liu X, Wang K: **iCAGES: integrated CAncer GEnome Score for comprehensively prioritizing driver genes in personal cancer genomes**. *Genome Med* 2016, **8**(1):135.
84. Hidalgo M, Amant F, Biankin AV, Budinska E, Byrne AT, Caldas C, Clarke RB, de Jong S, Jonkers J, Maelandsmo GM *et al*: **Patient-derived xenograft models: an emerging platform for translational cancer research**. *Cancer Discov* 2014, **4**(9):998-1013.
85. Izumchenko E, Paz K, Ciznadija D, Sloma I, Katz A, Vasquez-Dunddel D, Ben-Zvi I, Stebbing J, McGuire W, Harris W *et al*: **Patient-derived xenografts effectively capture responses to oncology therapy in a heterogeneous cohort of patients with solid tumors**. *Ann Oncol* 2017, **28**(10):2595-2605.
86. Villacorta-Martin C, Craig AJ, Villanueva A: **Divergent evolutionary trajectories in**

transplanted tumor models. *Nat Genet* 2017, **49**(11):1565-1566.

87. Eirew P, Steif A, Khattra J, Ha G, Yap D, Farahani H, Gelmon K, Chia S, Mar C, Wan A *et al*: **Dynamics of genomic clones in breast cancer patient xenografts at single-cell resolution**. *Nature* 2015, **518**(7539):422-426.
88. Willyard C: **The mice with human tumours: Growing pains for a popular cancer model**. *Nature* 2018, **560**(7717):156-157.
89. Wang M, Yao LC, Cheng M, Cai D, Martinek J, Pan CX, Shi W, Ma AH, De Vere White RW, Airhart S *et al*: **Humanized mice in studying efficacy and mechanisms of PD-1-targeted cancer immunotherapy**. *FASEB J* 2018, **32**(3):1537-1549.
90. Alexandrov LB, Nik-Zainal S, Wedge DC, Aparicio SA, Behjati S, Biankin AV, Bignell GR, Bolli N, Borg A, Borresen-Dale AL *et al*: **Signatures of mutational processes in human cancer**. *Nature* 2013, **500**(7463):415-421.
91. Onitilo AA, Engel JM, Greenlee RT, Mukesh BN: **Breast cancer subtypes based on ER/PR and Her2 expression: comparison of clinicopathologic features and survival**. *Clin Med Res* 2009, **7**(1-2):4-13.
92. Cerami E, Gao J, Dogrusoz U, Gross BE, Sumer SO, Aksoy BA, Jacobsen A, Byrne CJ, Heuer ML, Larsson E *et al*: **The cBio cancer genomics portal: an open platform for exploring multidimensional cancer genomics data**. *Cancer Discov* 2012, **2**(5):401-404.
93. Enright AJ, Van Dongen S, Ouzounis CA: **An efficient algorithm for large-scale detection of protein families**. *Nucleic Acids Res* 2002, **30**(7):1575-1584.

Figures and Tables

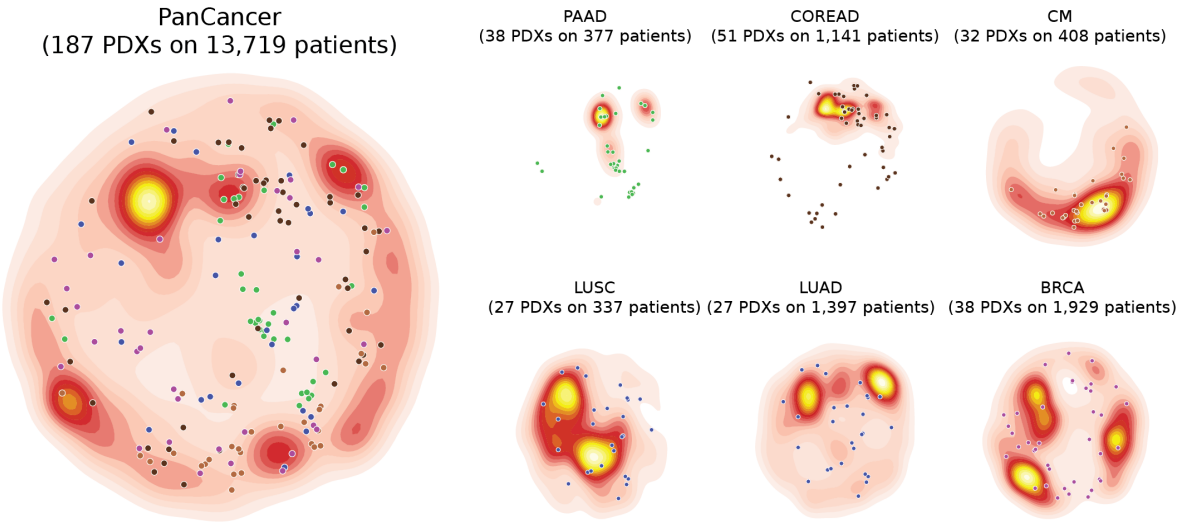

Figure 1. *Molecular representativity of PDXs. OncoGenomic Landscape* 2D representations of the molecular heterogeneity of the 187 PDXs annotated with both drug response data and oncogenic alterations, compared with that of their corresponding reference cohorts of cancer patients from TCGA and MSKCC. The points represent the location of each individual PDX, colored by tumor type. The distribution of the 187 PDXs can be compared to the distribution of patient samples, represented as density color-scale map in the background. PanCancer (n=15,212), BRCA (breast cancer, n=2,021), CM (cutaneous melanoma, n=492), COREAD (colorectal carcinoma, n=1,442), LUAD (lung adenocarcinoma, n=1,486), LUSC (lung squamous cell carcinoma, n=352), PAAD (pancreatic adenocarcinoma, n=442). Non-small cell lung cancer PDXs were mapped on top of both LUSC and LUAD reference populations.

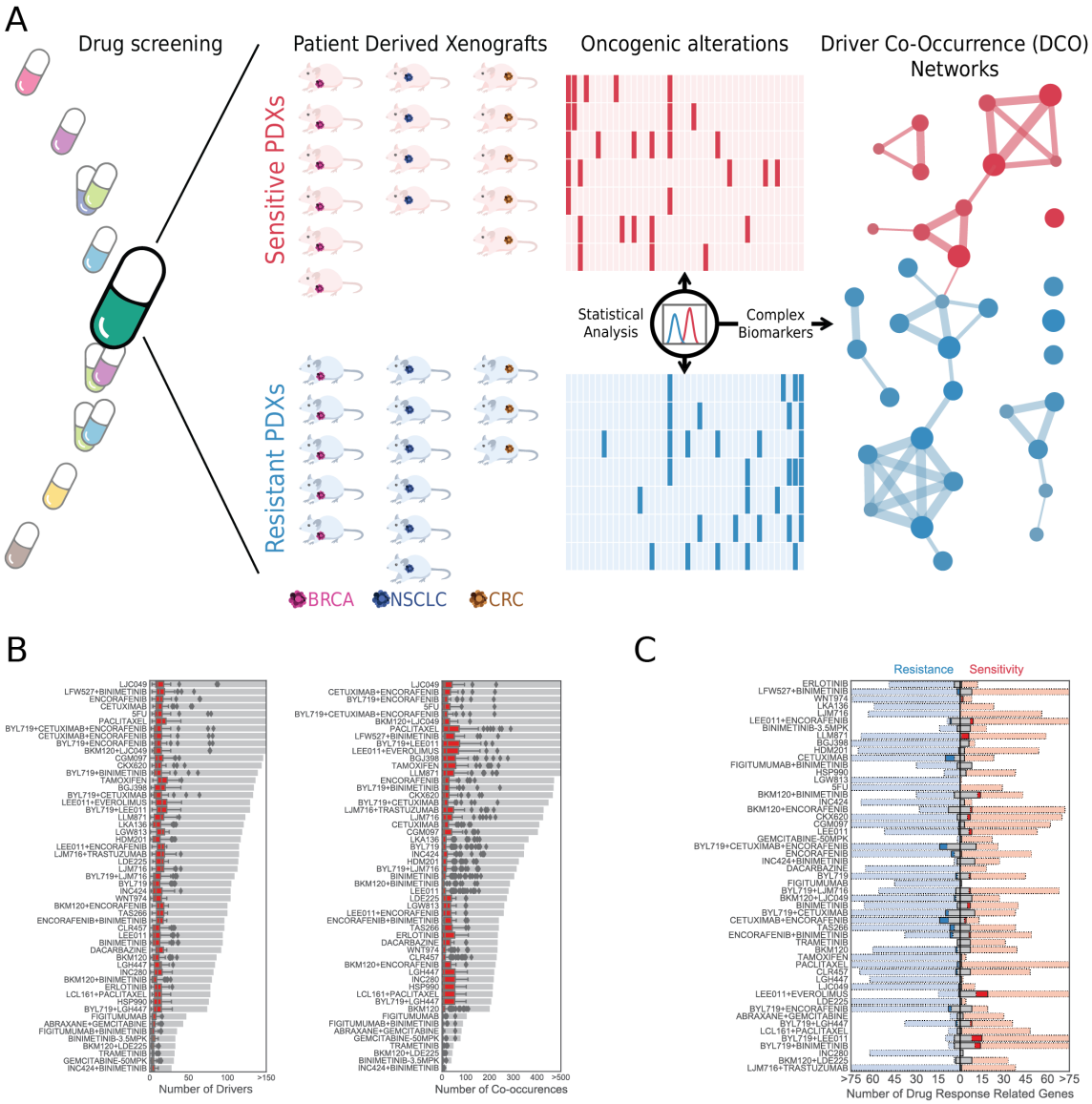

Figure 2. *Computational strategy and description of Driver Co-Occurrence (DCO) networks.* **(A)** We inferred DCO networks from the analysis of 3,127 *in vivo* experiments that screened the efficacy of 53 treatments against a panel of 187 molecularly characterized PDXs of several tumor types. We first compared the patterns of oncogenic mutations and CNVs. in sensitive and resistant PDXs, regardless of the tissue of origin of the tumors. Next, we identified sets of driver genes showing differential alteration rates between responders and non-responders (DiffD), which are represented as red or blue nodes in DCO networks, respectively. Additionally, we identified pairs of genes whose alteration co-occurred more often than expected given the alteration rate of each driver (Ps), and that did so more often in one of the two response groups. We represented each pair of co-altered drivers as two nodes connected by an edge. We derived a sensitivity, resistance and global DCO network for each treatment. **(B)** Gray bars show the number of drivers and pairs of co-occurring drivers included in each DCO network derived from whole exome sequencing data. Red boxplots show the distribution of the number of drivers or driver co-occurrences identified in each individual PDX. **(C)** Blue and red boxes represent the overlap between DCO drivers and genes with annotated biomarkers of resistance or sensitivity, respectively. We show in

light blue and light red the number of drivers in the resistance and sensitivity DCO networks that were not previously associated to drug response. Likewise, gray bars indicate the number of drug response associated genes that were not included in our DCO networks. In this analysis, we only considered as drug response associated those genes with biomarkers identified in two or more PDXs, which is a requirement that any driver needs to satisfy in order to be incorporated to a DCO network.

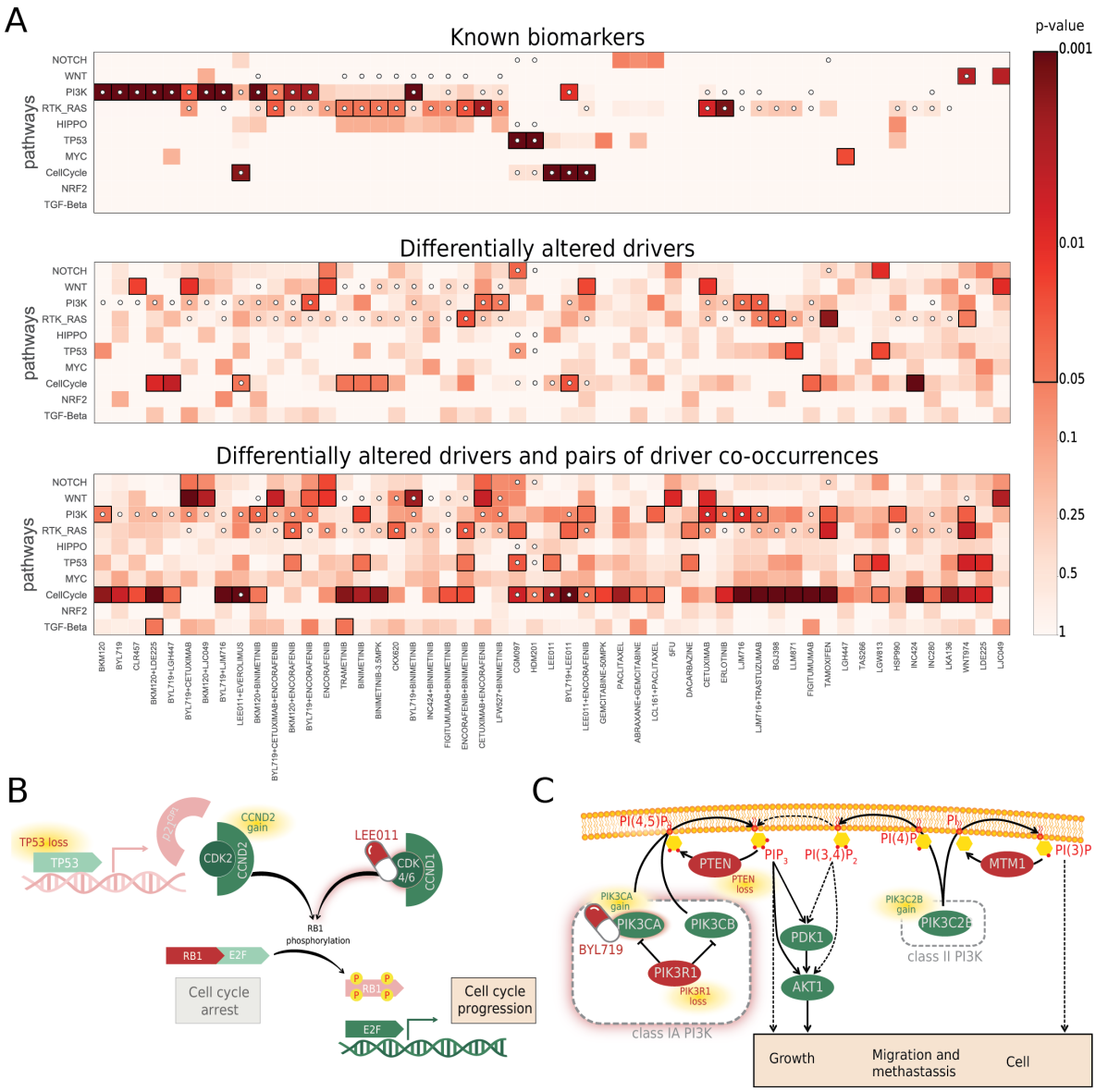

Figure 3. *Functional analysis of Driver Co-Occurrence (DCO) networks.* **(A)** The three heatmaps show the enrichment of 10 main oncogenic signaling pathways across the set of genes with FDA-approved biomarkers, the set of drivers with differential alteration rate between responders and non-responders (DiffD), and the whole set of drivers and pairs of drivers in the DCO networks (DiffD_DiP). Associations with a one-sided Fisher's Exact test p-value < 0.05 are squared in black. White circles denote the presence of at least one drug target in a pathway, which is informative of the mechanism of action of each treatment. This representation shows that reported biomarkers tend to be enriched in the same pathways they are directly targeting, whereas DCO networks expand beyond the drug target, with the potential to uncover more distant functional relationships. Cell cycle related proteins seem to play a central role in the DCO networks inferred for almost half of the treatments (35 of 53), irrespectively of the mechanism of action of the drug. **(B)** The DCO network of ribociclib, a CDK4/6 inhibitor, is enriched in cell cycle related proteins, such as CCND2, CCND3, CDKN2A, CDKN2B, CDK6 or RB1 (OR 6.54, p-value 0.0028; see Table S2). Based on the observed driver alteration co-occurrence patterns, we propose that the co-alteration

of TP53 and Cyclin D2 (CCND2) might abrogate CDK4/6 dependency, rendering tumors insensitive to ribociclib. More specifically, we hypothesize that TP53 loss would relieve CDK2 from the inhibitory activity of one of its major transcriptional targets, $p21^{CIP1}$. This would synergize with the gain of function of CCND2, which preferentially binds to and activates CDK2, facilitating an alternative CDK4/6-independent activation of G1/S transition. **(C)** The DCO network of alpelisib (BYL719), an isoform-selective PI3K inhibitor, includes four proteins that are involved in PI3K signaling: PIK3CA, PIK3R1, PIK3C2B and PTEN. Tumors that depend exclusively on PIK3CA for the activation of PI3K signaling respond well to this treatment (65.2% response rate), whereas tumors in which PIK3CA alteration co-occurs with either PIK3R1, PIK3C2B or PTEN alterations show a response rate very similar tot that of wild-type PIK3CA tumors (45.45% and 44%, respectively). PIK3C2B, a member of class II PI3K family, tends to be co-altered with PIK3CA more often than expected, and more frequently in resistant than in sensitive PDXs. PIK3C2B contributes to phosphatydil inositol signaling by phosphorylating the third position of the inositol ring, taking as substrates both phosphatidyl inositol and phosphatidyl-4-phosphate inositol. The resulting products might directly or indirectly contribute to cell survival, growth or metastasis in a PIK3CA-independent manner, which would represent a novel mechanism of resistance to PIK3CA inhibition.

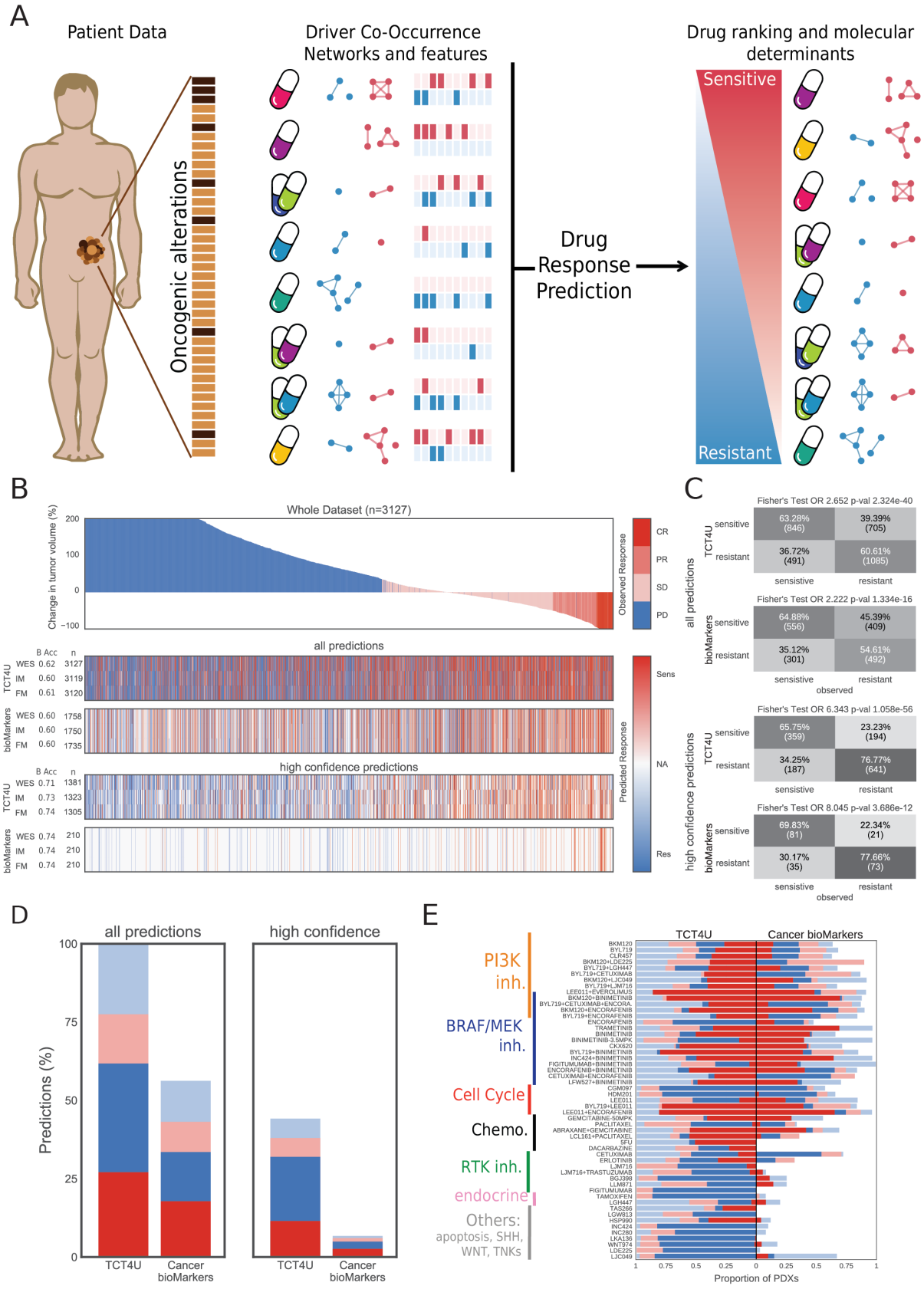

Figure 4. *Targeted Cancer Therapy for You (TCT4U), a collection of Naïve Bayes drug response classifiers based on DCO networks.* **(A)** Given a new tumor sample, we compare it to the patterns of driver alterations and co-alterations associated to sensitivity or resistance

to any of the treatments in TCT4U, and rank the drugs accordingly, predicting whether a drug will or not be effective. Since the number of driver alterations that tumors typically have is relatively small, we can know which are the molecular determinants used by the classifier and use this information for functional interpretation of the predictions. **(B)** Waterfall plot representation of the outcome of the *in vivo* pharmacogenomic screening used to infer our collection of DCO networks and TCT4U drug response classifiers. Each bar represents the best average response of one of the 3,127 *in vivo* experiments, sorted (left to right) from the worst to the best response to treatment, and colored according to the mRECIST classification as PD (progressive disease), SD (stable disease), PR (partial response) and CR (complete response), as proposed by [28]. The heatmaps below show the predictions of TCT4U in a leave-one-out cross validation setting and the predictions made on the basis of known biomarkers. Each heatmap has three rows, which correspond to the predictions obtained when examining the whole exome (WES) or a subsampled molecular profile containing the genes covered by MSK-IMPACT (IM) or Foundation Medicine (FM) targeted gene panels. The number of predictions and their balanced accuracy are annotated along the y-axis. The set of 'high-confidence' predictions refers, on the one hand, to the subset of 10 highest scoring sensitivity and resistance predictions per PDX, and to the subset of clinically approved biomarkers on the other hand. **(C)** Contingency tables showing the association between the observed and the predicted drug responses based on WES profiles. **(D)** The precision of each set of predictions is illustrated by the red and blue sections of the stacked bar plots, which represent the proportion of correct sensitivity and resistance predictions. Analogously, incorrect predictions are represented in faint colors. Missing predictions (NA) are represented in white to offer a comparative overview of the recall. **(E)** Stacked bar plots representing the precision and recall of all TCT4U predictions and all reported biomarkers, covered by WES profiles split by treatment arm.

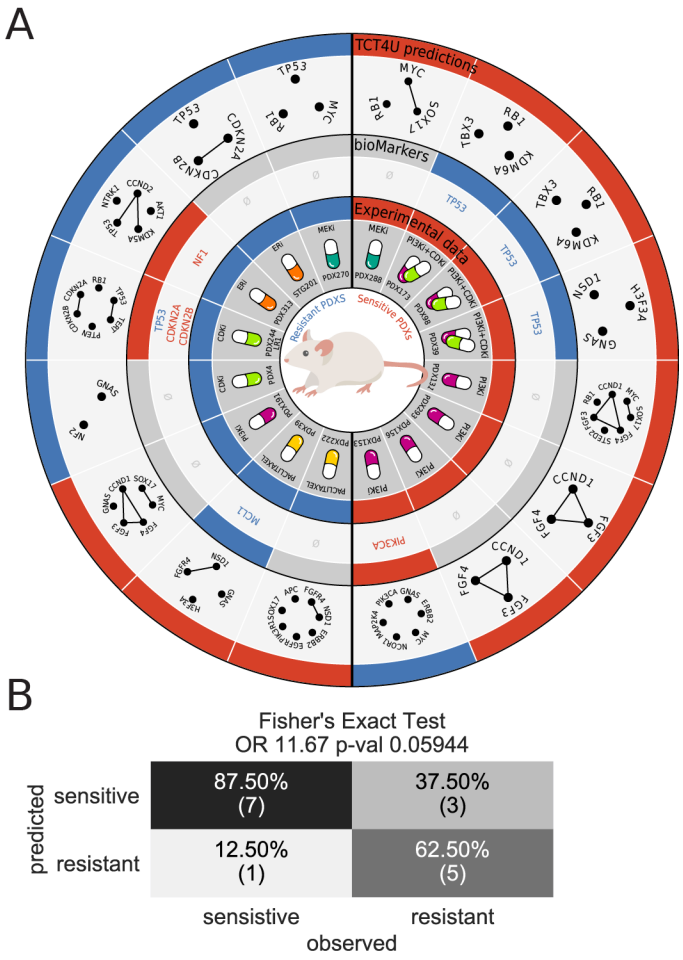

Figure 5. *In vivo validation of 16 high-confidence TCT4U predictions based on MSK-IMPACT profiles with missing or conflicting reported biomarkers.* **(A)** The circular plot summarizes the results of 16 *in vivo* experiments comprising 5 PDXs treated with the alpelisib (BYL719) isoform-selective PI3K inhibitor (PI3Ki), 2 PDXs treated with ribociclib (LEE011) CDK4/6 inhibitor (CDKi), 3 PDXs treated with the combination of both (PI3Ki+CDKi), 2 PDXs treated with binimetinib MEK inhibitor (MEKi), 2 PDXs treated with tamoxifen ER antagonist (ERi), and 2 PDXs treated with paclitaxel. The innermost track shows the experimentally determined treatment outcome, in which responder tumors showing disease stabilization or regression are represented in red, and non-responders are represented in blue. The middle track represents the predictions based on reported biomarkers and the genes to which they are annotated, when available. The outermost track represents the predictions based on TCT4U and their underlying molecular determinants. TCT4U predictions are sorted from correct to incorrect following clockwise and anticlockwise directions for sensitivity and resistance, respectively. **(B)** Contingency table showing the association between the observed and predicted responses to treatment.

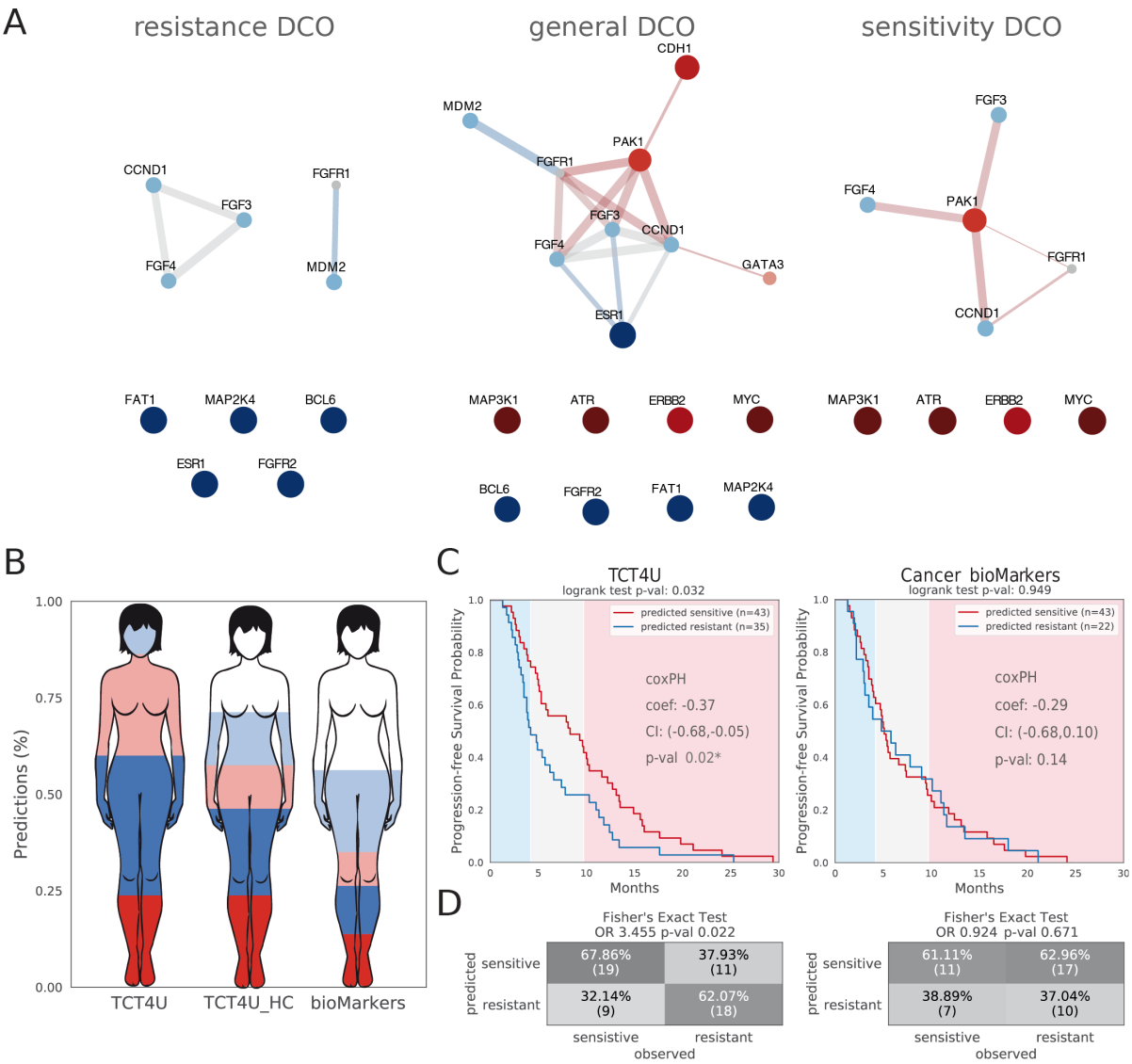

Figure 6. Application of TCT4U to predict treatment outcome in a clinical cohort of HR+/HER2- metastatic breast cancer patients. **(A)** Driver Co-Occurrence networks (DCO) representing the oncogenic alterations and pairs of alterations that are overrepresented in patients that relapsed early (resistant) or in in patients that derived a durable clinical benefit (sensitive) from CDK4/6 inhibition in combination with hormonal therapy combined with a. **(B)** Stacked bar plots representing the precision and recall of TCT4U cross-validated predictions and that of approved and experimental biomarkers. The blue and red sections of the stacked bar plots represent the proportion of correct predictions, in terms of the classification into early or late relapse. Analogously, incorrect predictions are represented in faint colors. Missing predictions are represented in white, offering a comparative overview of the recall. **(C)** Kaplan-Meier analysis of progression free survival (PFS). TCT4U high-confidence predictions are better able to discriminate between patients that would experience early and late relapse than known biomarkers, with a median time to progression of 4.2 and 8.3 months respectively (log-rank test p-value 0.03 and Cox's PH coefficient of -0.37, p-val 0.02). **(D)** The contingency tables show the concordance between observed and predicted clinical benefit.

Supplementary Data

Supplementary Table S1. *DCO Networks*. This dataset contains the whole collection of TCT4U DCO networks. The Nodes Table contains the information about each individual gene in each DCO network it participates in. We provide information about the specific treatment arm from which the DCO network was inferred (drug), the number of sensitive and resistant PDXs with and without driver alterations in it (mut_sens, mut_res, no_mut_sens, and no_mut_res), the estimated probability that the alteration rate is higher in resistant than in sensitive (DiffD), and the two-sided e-value associated to it (DiffD e-val). We also provide the chromosomal location of each gene (chrom, chromStart, and chromEnd), together with the genome adjacency clusters it has been assigned to in the global, sensitivity and resistance DCO networks (global_mcl, sens_mcl, and res_mcl), if any. We also indicate whether a given gene is covered by MSK-IMPACT and FoundationMedicine targeted gene panels. The three accompanying Edge Tables (global, sensitivity, and resistance) describe the pairs of drivers (prot1 – prot2) that appear co-altered more often than expected in each of the three DCO networks inferred from a treatment arm (drug). We provide information about the number of sensitive and resistant PDXs with and without a given pair of co-occuring driver alterations in (coocurr_sens , coocurr_resist, no_cooccurr_sens, no_cooccurr_resist), the estimated difference between the observed and expected co-alteration rate (Ps), and the e-value associated to it (Ps e-val). We also indicate whether a given pair co-occurs more often in sensitive than in resistant PDXs (Ps_diff), whether the pair represents a within-cluster co-alteration (Genomic_Linkage), and their Mutual Information content (MI).

Supplementary Table S2. *DCO Functional Analysis.* The tables show the results of the functional enrichment analysis of the set of approved and experimental biomarkers, the set of differentially altered drivers (DiffD), and the set of genes considered in all the DCO networks (DiffD_DiP) inferred from each treatment. We also report the results of the same analysis performed separately for sensitive (sensDiffD, sensDiffD_DiP) and resistance DCO networks (resDiffD, resDiffD_DiP). We report the contingency tables, the Odds Ratio (OR) and the nominal p-value of a one-sided Fisher's exact test, and the list of genes in the intersection. We used as gene universe the set of 58 genes with annotated biomarkers on one hand, and the set of 676 genes with detected driver alterations in the dataset, on the other hand.

Supplementary Table S3. Summary of the experimental validation of 16 high confidence TCT4U drug response predictions that were not in agreement with approved or experimental biomarkers. For each drug-PDX pair we report the anticipated response according to approved or experimental biomarkers (bioMarkers db) or by TCT4U, together with the experimentally determined response. Drug-PDX pairs were classified following the mRECIST criteria into responders (SD, PR or CR) and non-responders (PD). Additionally, we report the time at which the Best Response was observed and the tumor growth achieved at this time point with respect to the baseline, both in the treatment and placebo arms. We also provide the tumor growth inhibition in the treatment arm with respect to the placebo.

Supplementary Table S4. *Clinical and molecular profile (Mutations and CNAs) of a cohort of 216 advanced metastatic breast cancer patients treated with a CDK4/6 inhibitor in combination with an aromatase inhibitor at the Memorial Sloan Kettering Cancer Center (MSKCC).* We report the somatic mutations and copy number alterations detected in pre-treatment biopsies of the tumors using MSK-IMPACT gene panel. Genomic data has been annotated using MSKCC knowledge base database (OncoKb REF) and also with clinical data indicating the line of therapy (txline), the time to progression in months (pfsm), and the outcome variable (pfs_event), which takes a value of 1 when the treatment was discontinued because of tumor progression or a value of 0 for other causes of discontinuation such as toxicity, medical doctor decision or decease.

Supplementary Table S5. *TCT4U drug family annotation.* Mapping of TCT4U drugs to drug families and drugs for which we could identify at least one approved or experimental biomarker of response reported in the Cancer bioMarkers database accessed in the 25th of August 2017.

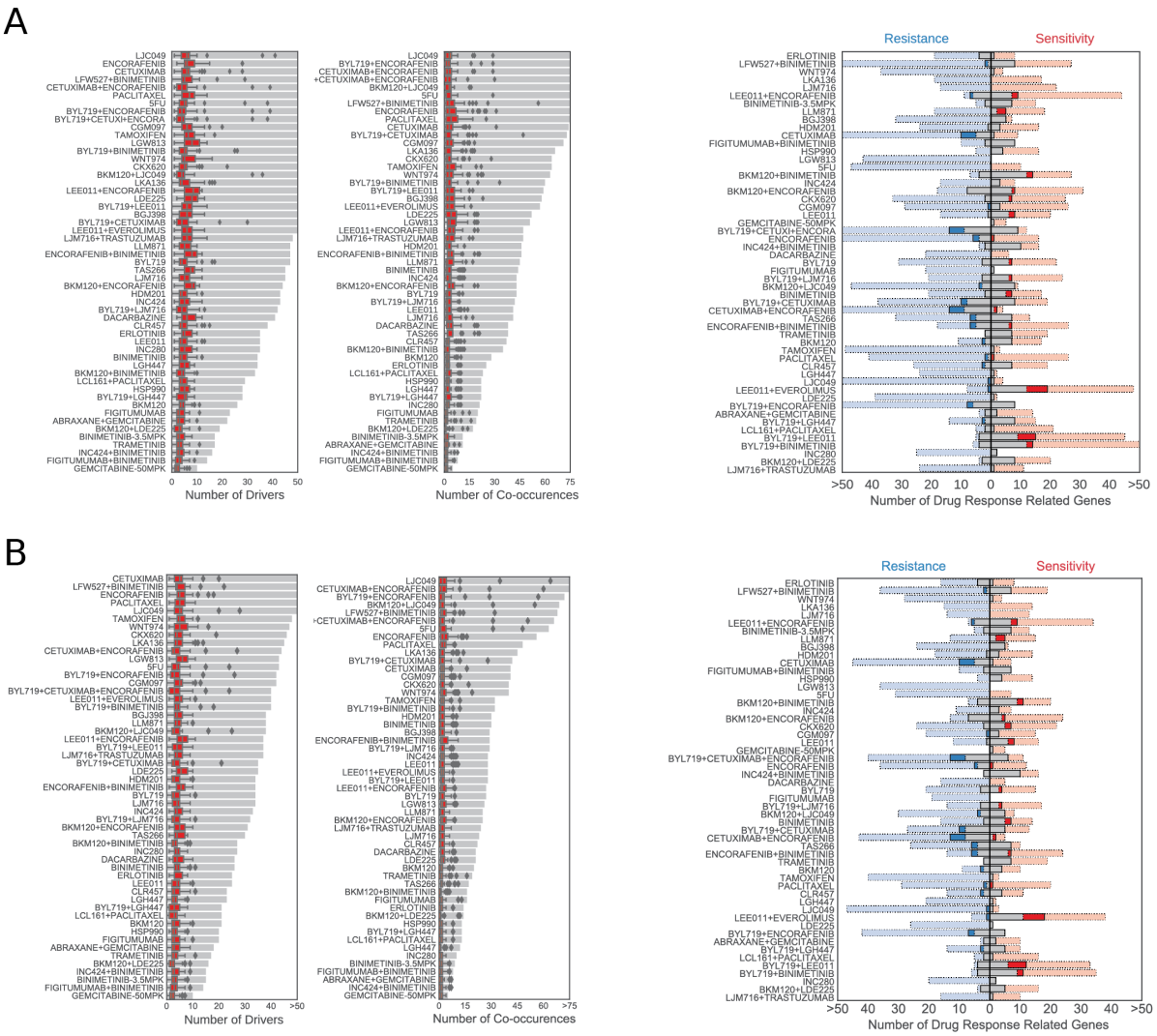

Supplementary Figure S1. *Characterization of the DCO networks derived from targeted gene panels*. **(A)** DCO networks derived from MSK-IMPACT gene panel have 10 to 79 driver genes (median of 47, IQR: 34-57) and 5 to 230 pairs of drivers (median of 45, IQR: 25-64). Each PDX has a median of median of 5 altered drivers (IQR: 3-7) and 2 driver alteration co-occurrences (IQR: 1-4). **(B)** DCO networks derived from Foundation Medicine gene panel have 10 to 56 driver genes (median of 34, IQR: 23-42) and 5 to 85 pairs of drivers (median of 27, IQR: 16-40). Each PDX has a median of 4 altered drivers (IQR: 2-5) and 1 driver alteration co-occurrence (IQR: 0-3).

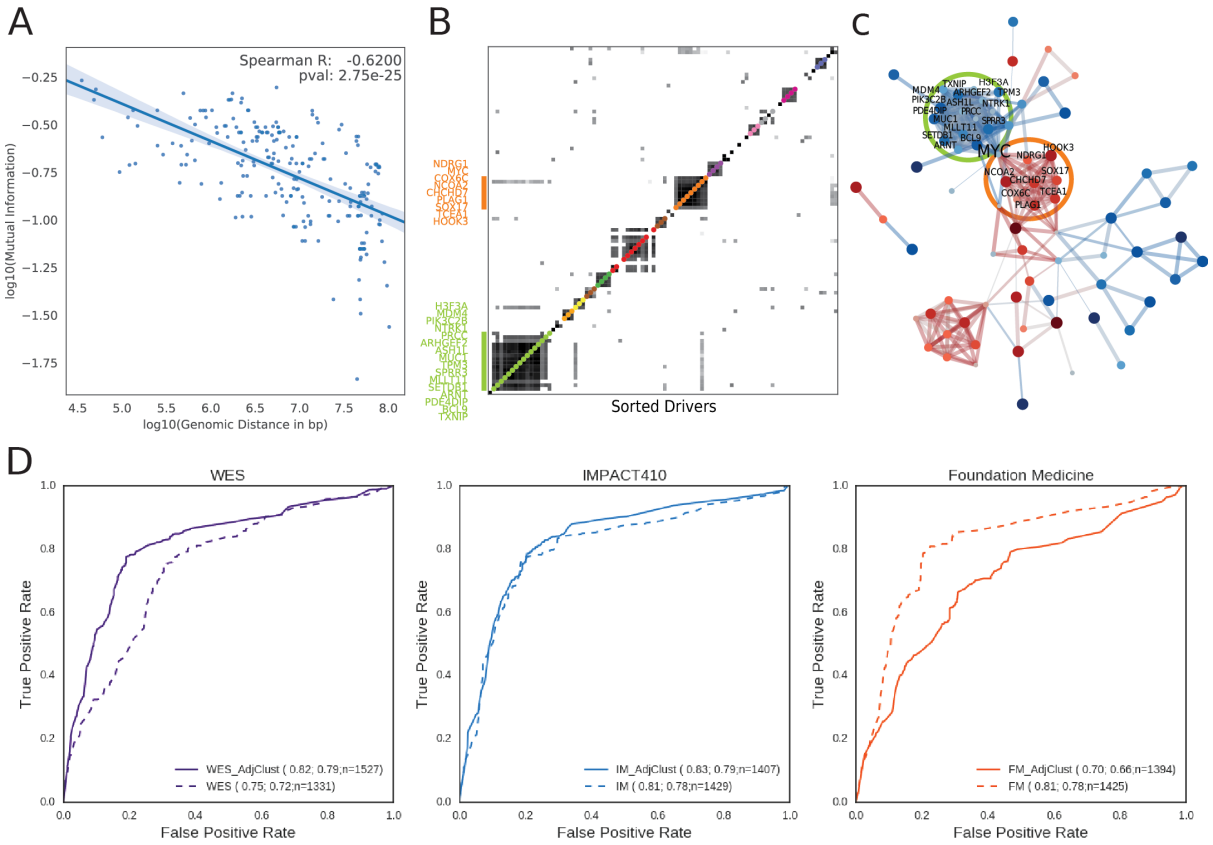

Supplementary Figure S2. *Genomic linkage in whole exome sequencing profiles.* As an illustrative example, we show the genomic linkage of driver genes considered in binimetinib (MEK inhibitor) DCO network. **(A)** Correlation between pairwise mutual information content (MI) with respect to genomic distance of intra-chromosomal pairs of drivers. **(B)** Heatmap representation of mutual information content of pairs of drivers sorted by genomic coordinates. The different colors indicate the labels of a MCL clustering of adjacent drivers with high MI. Highlighted genes belong to two large clusters that tend to be co-altered with MYC. **(C)** Partial view of binimetinib DCO network, showing the pivotal role of MYC alteration, which is associated with sensitivity when co-altered with its adjacent genes in chr8 p11-12 and chr8 q11-24 (orange cluster), or with resistance when co-altered with a cluster of distant genes that are mostly located in chr1 q21-23 region. **(D)** Adjusting for genomic linkage improved the overall performance of the whole exome sequencing (WES) derived models, had very little impact on MSK-IMPACT derived models, and worsened the performance of Foundation Medicine derived models.

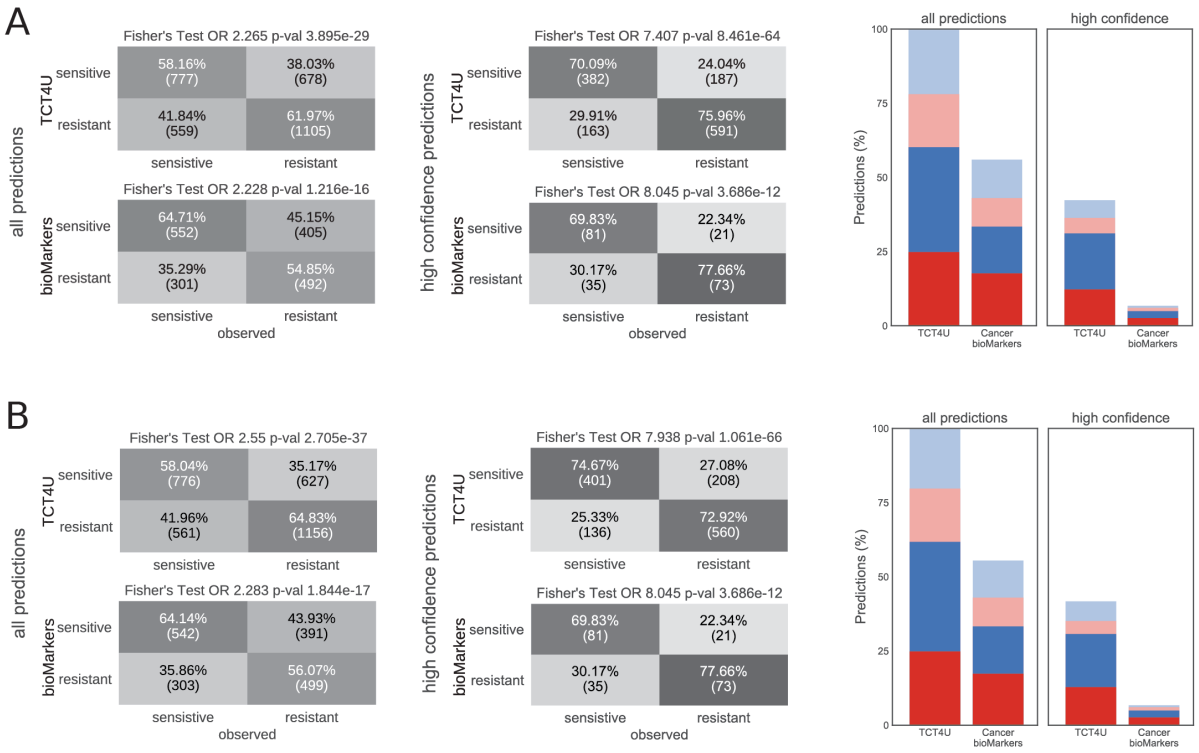

Supplementary Figure S3. *Evaluation of TCT4U models derived from the subset of alterations that would be detectable by two widely used targeted gene panels.* ***(A)*** *MSK-IMPACT* [51] *and* ***(B)*** *Foundation Medicine* [53]*.* The contingency tables show the association between the observed and the predicted drug responses. The precision and recall of each set of predictions is illustrated by the red and blue sections of the stacked bar plots, which represent the proportion of correct sensitivity and resistance predictions. Analogously, incorrect predictions are represented in faint colors. Missing predictions are represented in white to offer a comparative overview of the recall.